

H. DEVELOPMENT OF NEW EXPERIMENTAL EQUIPMENT

New techniques and new approaches drive the field of nuclear physics forward. It is encouraging that the current year has been very rich in equipment developments. In almost all our experimental areas new projects are emerging that offer unparalleled opportunities for the future.

h.1. Target Laboratory Developments (J. P. Greene)

The target development laboratory is a key component of our research that produces targets and foils of various thicknesses and substrates, depending on the requirements, for experiments performed at ATLAS. The targets are prepared from both naturally occurring materials and stable isotopes that are supplied either in pure, elemental form or as stable compounds. In addition to ATLAS experiments, targets and foils are provided for all staff members whether working within the Physics Division or undertaking experiments at other facilities, for instance, the Advance Photon Source (APS). Also, wherever possible, support is provided to other ANL Divisions, and in particular to requests from researchers at the University of Chicago. Numerous collaborations have grown out of efforts between the Physics Division and target laboratory staff with outside groups in order to provide targets.

In the past year, numerous targets were fabricated either as self-supporting foils, on various substrates or as "sandwich" targets. Targets produced included Ag, Al, Au, ^{10}B , BN, ^{12}C , ^{40}Ca , ^{106}Cd , ^{141}Ce , ^{50}Cr , ^{54}Fe , Havar, ^{180}Hf , $^{92,94,100}\text{Mo}$, Mylar, Nd_2O_3 , ^{58}Ni , ^{208}Pb , $^{108,110}\text{Pd}$, Polycarbonate, Pt, ^{28}Si , ^{112}Sn , Ta, $^{128,130}\text{Te}$, Teflon, Th, ThF_4 , ^{46}Ti , ^{234}U , UC_2 , UF_4 , Valine, Y, and ^{176}Yb . Many of these target foils have been fabricated via mechanical rolling using our small rolling mill. During 2004, approximately 528 targets were prepared for various experiments.

Efficient Gammasphere operation has prompted an increase in demand for various targets and sources prepared by the target laboratory. For the past calendar year, 237 targets were prepared for experiments using Gammasphere.

Beyond target development, the production of thin plastic films and foils for use in various detector systems and energy degraders needed for the CPT and for astrophysics research continues.

As part of ATLAS accelerator support, the target lab routinely produces carbon stripper foils of $2\ \mu\text{g}/\text{cm}^2$ for use in the Tandem Van de Graff as well as other thickness for additional stripping throughout the accelerator. Over 233 carbon stripper and gold foils of various types were prepared for ATLAS during this past year. There continues to be an increase in the preparation of various dilutions of isotopic source material into a form and shape suitable for introduction into the ion sources for the production of enriched beams at ATLAS. These have included ^{64}Ni , $^{34,36}\text{S}$ and ^{50}Ti .

The target development laboratory includes state-of-the-art equipment used for thin-film fabrication. The addition of a new, multi-purpose, computer-controlled vacuum evaporation system extends our capabilities and provides a stable platform for the continued production of accelerator targets. The available techniques consist of multiple resistive heating, focused ion beam sputtering, ion assisted deposition, electron beam and electron bombardment evaporation, carbon arc evaporation, electrodeposition and mechanical rolling. The evaporators are maintained under high vacuum and each vessel contains a quartz-crystal film-thickness monitor with deposition rate indicators. Also included are movable shutters, quartz-lamp substrate heaters and thermocouple temperature sensors, allowing for complete process monitoring during target deposition.

Other auxiliary equipment used for target development includes electrodeposition apparatus, a small rolling mill, an alpha particle counting chamber, inert atmosphere glove box, laminar flow clean bench, pellet press, a reduction furnace, and a variety of precision balances. A turbo-pumped target storage facility is in operation for maintaining, under high vacuum, those targets that readily oxidize in air. This system utilizes computer-controlled circuitry to prevent targets from exposure to atmosphere during power interruptions. A second storage system employing a bank of vacuum desiccators and connected to a mechanically pumped manifold is available for use by individual experimenters. An additional set-up,

consisting of two large glass desiccators evacuated using a small turbo-pump system, is in operation for long-term material storage. This allows a separation of material storage from target storage, hence eliminating repeated exposure when transferring and retrieving targets.

A low-level radioactive source and target preparation laboratory exists at a separate location within the Division that is dedicated to the production of these sources and targets. Available preparation techniques include multiple resistive heating, employing a diffusion-pumped vacuum evaporator. A second, smaller evaporator system was constructed for close proximity evaporations of higher activity materials, to be used as targets as well as radioactive sources. The small size of this system allows for installation within a hood. Preparation and handling of ^{14}C targets as well as fission sources (mainly ^{252}Cf) by electrodeposition has been done in this lab for experimental studies at ATLAS as well as routine

rolling of natural U and Th foils.

Another area of increased research effort has been toward development of radioactive beams for the RIA proposal and involves neutron producing targets which in turn induce fission in uranium or a uranium compound production target. Toward this end, direct measurements of the thermal conductivity of uranium carbide have been made using the method of electron beam heating provided by a 10 kV mortar source in vacuum with the temperature measured as a function of beam current using a two-color pyrometer. Sample uranium carbide material of small grain size is being prepared in-house in collaboration with the ES Division in Building 212. This work is still in progress.

In August, the Physics Division hosted a RIA Summer School, which included a “hands-on” Accelerator Targets Session which gave students access to the target facility and target making techniques.

h.2. New Control System Hardware and Software for the FMA (C. N. Davids)

When the FMA was first put into operation in 1991, a control system using an Apple Macintosh II was written in Borland’s Turbo Pascal, taking advantage of the Macintosh graphical user interface. Communication between the computer and the FMA ion-optical devices, power supplies, and vacuum sensors was accomplished via an RS-232 serial link. However, after several years, Turbo Pascal for the Macintosh was discontinued, thus freezing the development environment. Many surplus Macintosh II computers were stockpiled for replacement parts,

but as aging and obsolete hardware began to cause reliability problems, replacement of the control software and hardware finally became a necessity. New software for the FMA control system has been written using REALbasic, an object-oriented program development environment for Macintosh, Microsoft Windows, and Linux. The program utilizes the existing serial communication link, and the user interface was made identical to the Pascal version. The new program is now in regular use, with backups and development being done on a separate identical computer.

h.3. The Isobar Separator Ion Trap for the APT and CPT Trapping Systems (G. Savard, N. D. Scielzo, J. A. Clark, J. Fallis, J. Guest, S. Gulick, A. A. Hecht, A. Levand, B. Lundgren, B. Nardi, H. Sharma, K. S. Sharma, M. Sternberg, I. Tanihata, A. Villari, J. Wang, Y. Wang, Z. Zhou, and B. J. Zabransky)

The Advanced Penning Trap (APT) System consists of two newly constructed ion traps – a Penning Trap “Isobar Separator” for the purification of ion samples and an RFQ “Decay Trap” that will be used to study radioactive decays. These new traps will expand the ion trapping capabilities on the Canadian Penning Trap (CPT) mass spectrometer beamline.

The Isobar Separator will deliver extremely pure samples of radioactive ions to the RFQ Decay Trap

for decay studies or to the CPT mass spectrometer to extend its reach to even more weakly-produced and short-lived species. With a magnetic field of 6.83 T, the Isobar Separator will ultimately be able to obtain mass resolutions ($\Delta m/m$) of 10^{-5} and will allow removal of unwanted isobars from ion samples by applying weak RF electric fields at the appropriate cyclotron frequencies.¹ In 2004, the superconducting magnet was shimmed and the titanium vacuum tube used to host the trap installed and lined up on the magnetic field axis using collimated

electron beams. The trap was installed together with the gas feeding system. The ion optics elements used to transfer ions from the existing CPT ion injection

system to the Isobar Separator were designed, constructed, and assembled in the Triangular Room (see Fig. I-64).

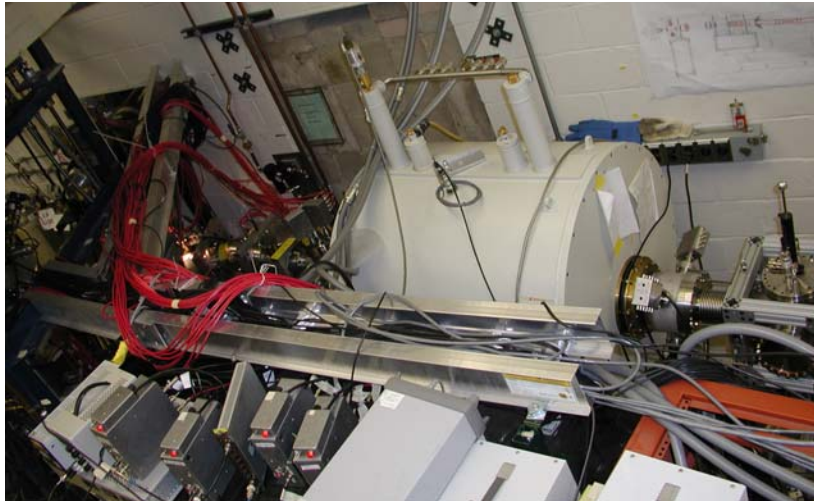


Fig. I-64. Photo of the isobar separator ion trap magnet in location in the triangular room and of the transfer lines feeding ions into and out of it. After cooling and mass separation, the purified- ion sample can either be sent back towards the CPT mass precision trap or be transported (to the right on the figure) to the APT decay trap.

While loading ions into the RFQ Trap should be straight-forward, directing ions back to the CPT requires ejecting ions from the Isobar Separator in the direction from which they entered. The electronics needed for the required rapid control of the beamline flow is nearly completed. In addition, the MCP and Silicon detector diagnostics used to optimize ion transport have been designed to accommodate the bi-direction ion flow. The diagnostic detectors are located off-axis at 90° from the ion flow direction.

By applying the appropriate electric potentials to a quadrupole deflector, the ion beam can be directed to either detector while moving either towards the isobar separator or coming back from it. Using these diagnostics, ions were loaded into the isobar separator, and with the injection of He gas into the trap, the cooling and centering frequencies for various contaminants have been determined. Optimization of the mass resolution and efficiency in the isobar separator ion trap is ongoing.

¹G. Savard *et al.*, Phys. Lett. **A158**, 247 (1991).

h.4. A Solenoid Spectrometer for Reactions in Inverse Kinematics (B. B. Back, C. J. Lister, K. E. Rehm, J. P. Schiffer, S. J. Freeman,* and A. H. Wuosmaa†)

The study of the structure of short-lived nuclei can often be studied only with reactions in inverse kinematics, such as transfer reactions. This poses severe experimental problems that are difficult to overcome. A magnetic device has been discussed (see ANL Physics Division Annual Report, 2003 p. 96) that would overcome many of the difficulties encountered by the large arrays of Si detector telescopes that are used at present.

During the last year the technical and operating aspects of the device have been investigated. A

construction site was chosen in the general purpose area, which can receive both stable and radioactive beams. A cost and effort breakdown has been made. In early 2005 a formal proposal was submitted to the DOE Office of Nuclear Physics for the construction of such a device.

In developing the science case for such an instrument a workshop was conducted and several scientists made contributions to the proposal, in addition to the names on this report. They included: Dr. L. Ahle (LLNL), Dr. K. L. Jones (Rutgers), Dr. A. O. Macchiavelli (LBNL), and Professor A. Champagne (North Carolina).

A more detailed design is being carried out and options for conducting a set of test measurements in a

“demonstrator” project have been investigated.

*University of Manchester, United Kingdom, †Western Michigan University.

h.5. A New Focal-Plane Detector System at the Argonne Fragment Mass Analyzer for Low Fusion-Evaporation Cross Section Measurements (C. L. Jiang, D. J. Henderson, D. Seweryniak, I. Tanihata, K. E. Rehm, C. N. Davids, D. Peterson, B. B. Back, J. P. Greene, R. V. F. Janssens, C. J. Lister, R. C. Pardo, T. O. Pennington, B. Shumard, S. Sinha, X. D. Tang, S. Zhu, P. Collon,* S. Kurtz,* and M. Paul†)

A recent program at the ATLAS facility has begun to study and characterize a new hindrance phenomenon at extreme sub-barrier energies for heavy-ion fusion reactions.¹⁻³ In order to study this behavior to very low cross sections, a new focal-plane detector system has been designed and constructed with the Fragment Mass Analyzer (FMA).

The new detector system has a modular structure configured as:

PGAC-TIC-PGAC-TIC-PGAC-IC,

where PGAC stands for an x - y position-sensitive parallel grid avalanche counter⁴, TIC for a transmission ionization chamber⁵ and IC for a large volume multi-anode ionization chamber.⁶ The first PGAC is mounted at the x focal-plane of the FMA. The three PGACs measure the position sets (x_1, y_1) , (x_2, y_2) , and (x_3, y_3) . Time-of-flight (TOF) measurements, t_2 and t_3 , between PGAC₁-PGAC₂ and PGAC₁-PGAC₃, are also recorded. The ionization chambers provide seven ΔE signals: ΔE_1 - ΔE_4 from the two TICs (two each), and ΔE_5 - ΔE_7 from the IC. Another TOF signal, t_{rf} , measures the time difference between the accelerator radio frequency (RF) and the first PGAC. Each of the three PGACs also provides a ΔE signal. These measurements provide a rich data set from which excellent separation of desired signals over background has been obtained. The three PGACs and the two TICs share a common gas volume and are operated at a pressure of 3 Torr of isobutane. The last ionization chamber had an adjustable pressure of 22-30 Torr of isobutane. The gas pressures in both volumes were regulated to better than 0.05 Torr. A mylar foil of 0.12 mg/cm² served as the entrance window to the first PGAC. A second mylar foil of 0.22 mg/cm² thickness separated the third PGAC from the last ionization chamber.

At low energies, the fusion evaporation residues often concentrate into only one or two masses and the element separation is generally unimportant. Full tracking of each event, using all of the signals measured in the detector system, is a good way to identify residues, but this can be rather tedious. A simpler method is desirable. In most cases a single, appropriate two-dimensional plot allows for the identification of evaporation residues at moderately low cross sections. Full tracking is required only at the lowest cross sections, where there are very few events.

Previous excitation function measurements at the FMA have found that pile-up from the E or ΔE signals is often the main background, even when pile-up rejection electronic circuits are used, because the counting rates are often very high in these low level cross sections experiments with most events originating from scattered beam. On the other hand, the pile-up behavior of the time-of-flight signal is different; it does not result in "peak summing". A rather successful residue-background separation method often employed was a two-dimensional plot of ΔE (or E) versus TOF. On that basis, the new design incorporates more TOF signals, longer flight paths, and tracking capability. Some performances of the present detector in an experiment $^{64}\text{Ni} + ^{100}\text{Mo}$ will be described. The experimental results of the excitation function are published in Ref. 7.

A set of x_i spectra at PGAC₁, PGAC₂ and PGAC₃ from a measurement at $E_{lab} = 245.8$ MeV, gated on only two masses, $m = 160$ and $m = 161$, are shown in Fig. I-65. The FMA was set for $q_0 = 25.5$ and $m_0 = 160$. Thus two charge states, $q = 25$ and 26 , were measured simultaneously. The PGAC₁ (m/q) spectrum is shown in (a), PGAC₂ spectra for $q = 25$ and $q = 26$ are shown in (b) and (d), and PGAC₃ spectra for $q = 25$ and $q = 26$ are shown in (c) and (e), respectively.

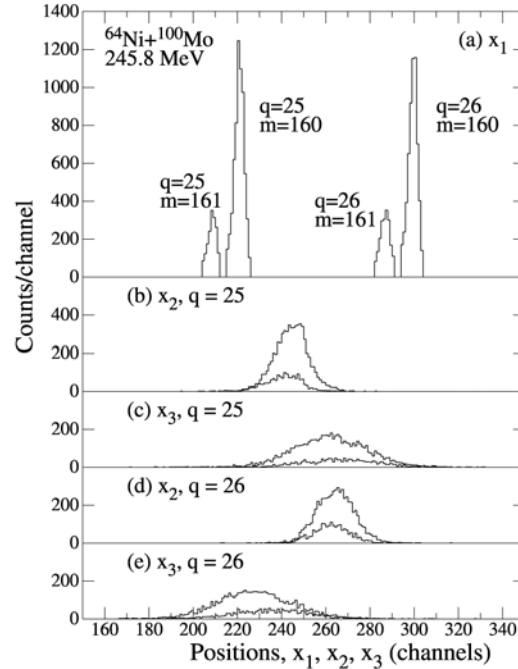


Fig. I-65. Measured x -tracking for the case mentioned in the text. x_1 , x_2 , and x_3 are measured at the three PGACs. Two masses and two charge states are shown for x_1 (a). Also shown is the evolution to x_2 and x_3 for the low charge state peaks ((b) and (c)) and high charge state peaks ((d) and (e)). Higher yield lines are for mass 160, and lower yield lines for mass 161, respectively. See text for details.

These position signals, at the three PGACs, constitute one kind of position-tracking for the present detector system. Another way to illustrate the position tracking behavior is with an x_1 - x_2 - x_3 plot. For each event, the measured values x_1 , x_2 and x_3 are used as ordinates and the values 100, 200 and 300 are respectively assigned to x_i along the abscissa. The three points of each event are then connected by

lines. An example is presented in Fig. I-66. In this figure, only 100 events with mass, $m = 161$, and two charge states, $q = 23$ and 24 , are shown. Good residue events are shown as dashed lines. Also shown in this figure are some dark, solid lines from background events that can be easily discriminated. It should be noted that this measurement corresponds to a low cross section level of ~ 300 nb.

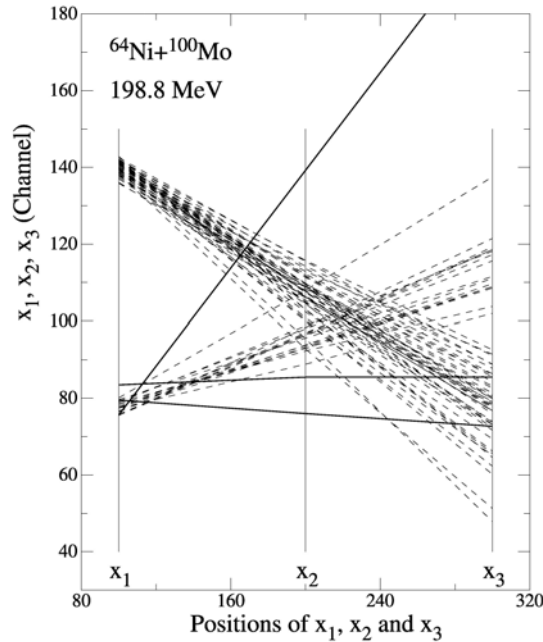


Fig. I-66. An x_1 - x_2 - x_3 tracking plot for $E_{lab} = 198.8$ MeV. The dashed lines are tracks due to evaporation residues: $m = 161$, $q = 23$ (smaller x_1) and 24 (larger x_1), respectively. The three dark solid lines are due to background events.

In order to show the resolution of the x_i determinations, a one dimensional plot dx is shown in Fig. I-67 for the same measurement at $E_{lab} = 245.8$ MeV. The quantity dx is defined as $x_2 - (x_1 + x_3)/2$, since the distances from PGAC₁ to PGAC₂ and PGAC₂ to PGAC₃ are the same. For clarity, only the group $m = 160$ and $q = 26$ is given. The FWHM of

the dx spectrum is 5.3 channels that corresponds to a x_2 peak centered at channel 265.8, with a x_i resolution of about $\pm 1\%$.

The y -tracking behavior is similar to the x -tracking and can be used as an auxiliary tool, though the y_i resolutions are poorer than the x_i resolutions.

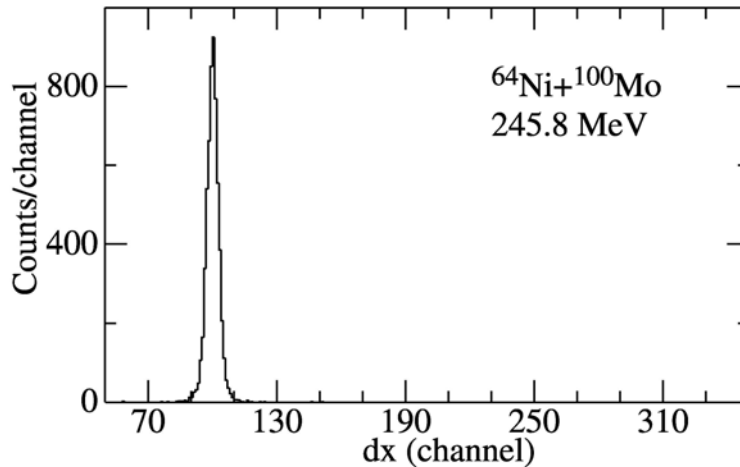


Fig. I-67. Illustration of x -tracking resolution for $q = 26$ and $m = 160$ in a measurement for $E_{lab} = 245.8$ MeV. The abscissa is defined as $dx = x_2 - (x_1 + x_3)/2$.

For our detector system each of the seven ΔE signals, $\Delta E_1 - \Delta E_7$ and their combinations (sums), together

with each of the two time-of-flight signals, t_2 and t_3 , can form a two-dimensional ΔE - t spectrum. In Fig. I-68, six

$\Delta E_i - t_3$ spectra are compared from a measurement at $E_{lab} = 211.8$ MeV. The ΔE_7 versus t_3 plot is not shown because, in this measurement, the gas pressure in the last ionization chamber was too high (30 Torr) and many residues produced only small signals in the ΔE_7 region. In each plot of Fig. I-68 there is a region originating from the evaporation-residues, which is indicated in Fig. I-68d as an example. The other

events are due to background. Obviously, as different particles pass from the focal-plane (PGAC₁) downstream to the last IC chamber, their ΔE_i behavior is different. In this case, ΔE_i signals from the background decreased more rapidly than the corresponding signals for residues as they moved away from the focal-plane. The separation between the residues and the background is best in the $\Delta E_6 - t_3$ spectrum.

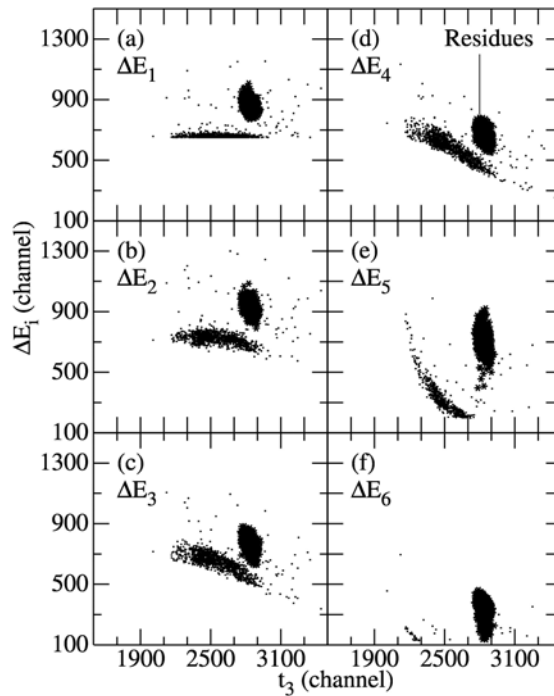


Fig. I-68. Two-dimensional ΔE_i vs. t_3 spectra, measured at $E_{lab} = 211.8$ MeV. The gas pressure in the IC was 30 Torr. The region in the right part of each plot is due to evaporation residues, which is marked in (d). All other events are background. In (a), only part of the background events are shown (a ΔE_1 cut appears).

In Fig. I-69, three plots of ΔE_i vs. t_2 and ΔE_i vs. t_3 are compared for a measurement at $E_{lab} = 205.1$ MeV (the gas pressure in IC was 22 Torr). There is good

separation of residues from background in all spectra, with $\Delta E_6 - t_3$ being the best choice, when using a single two-dimensional spectrum for residue identification.

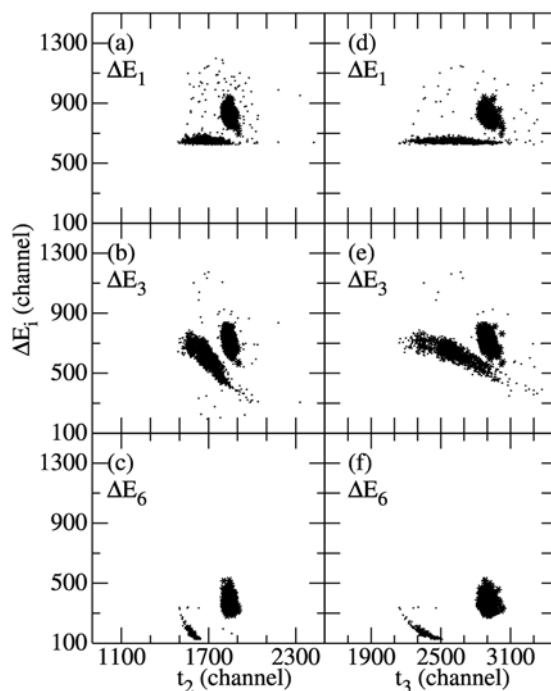


Fig. I-69. Comparisons of two kinds of two-dimensional spectra, $\Delta E_i - t_2$ and $\Delta E_i - t_3$, measured at $E_{lab} = 205.1$ MeV. The gas pressure in the IC was 22 Torr. The separations between evaporation residues and background are better with signal t_3 than with signal t_2 . Just as in Fig. I-68, ΔE_1 cuts were applied in Figs. I-68a and I-68b.

The seven ΔE_i signals (measured by the TIC or IC) effectively measure the Bragg curve of the particles. Figure I-70 illustrates such a curve obtained from a 245.8 MeV bombardment. The y-axis is the ΔE_i energy-loss per unit length and unit pressure ($\Delta E_i/\text{cm/Torr}$), and the x-axis follows the seven ΔE sections. The 100 dotted lines are due to the evaporation-residues and the 50 dashed ones originate from background. It can be seen that residue events and background events stop in different anode regions. In fact, Figs. I-68a-f display a similar behavior in the $\Delta E_i - t_3$ spectra. The circles inside the residue trajectories in Fig. I-70 are energy-loss calculations of the central tracks, normalized to

the measured data. Because residues stopped in the region of ΔE_7 , rendering the quantity $\Delta E_7/\text{cm/Torr}$ is meaningless, and the simulations are only shown for ΔE_1 to ΔE_6 . In this experiment, all residue energies are lower than the maximum of the Bragg curve so that the Bragg peak is not visible. Thus, the dE/dx measurements only show the increasing part of the Bragg curve. Background events from pile-up signals may have similar amplitudes for some ΔE_i signals, but it is highly unlikely that all of their ΔE_i signals would be similar to the residues. This provides yet another important tracking method that can be used to suppress background contaminations. Other two-dimensional plots, such as t_2 versus t_3 and ΔE_i versus E , can also be helpful in identifying the background.

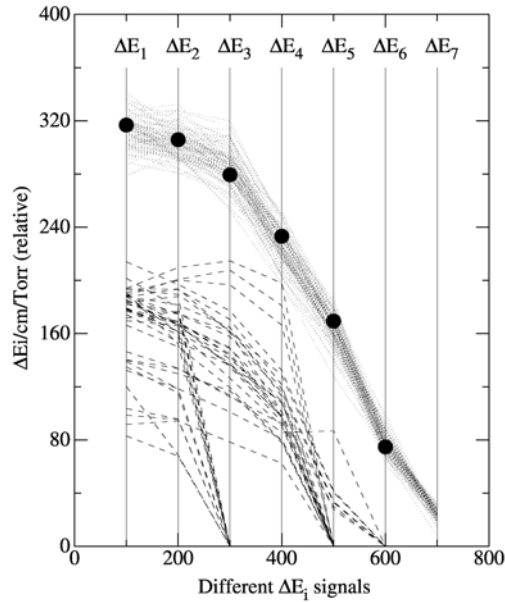


Fig. I-70. A Bragg curve spectrum obtained from seven ΔE_i signals. The y-axis is the energy lost per unit length and unit pressure ($\Delta E_i/\text{cm/Torr}$); the x-axis tracks the ΔE sections. The dotted lines indicate evaporation residues and the dashed lines indicate background. The filled circles are from calculations for the energy loss of an evaporation residue normalized to the measurement.

As mentioned above, the TOF from the longer flight distance, t_3 , combined with a ΔE signal measured far away from the focal-plane, (e.g. ΔE_6), yields the best separation between evaporation residues and background. The conditions during the commissioning experiment were chosen by assuming that some background particles would have longer ranges compared with the residues and enter the third anode region of the IC, while the residues stop in the second anode region of the IC. The third anode signal (ΔE_7) would then be used as a veto. During the experiment, however, it was found that the ranges of most background particles were less than the range of the residues. Thus, the pressure of this last IC was decreased to stop the residues in the last anode

region. Four plots of ΔE_6 versus t_3 , from measurements at different beam energies, are shown in Fig. I-71. The measured fusion-evaporation cross sections are 1.1 mb, 242 nb, <20 nb, and <4.6 nb, respectively. As in Figs. I-68 and I-69, the bands to the left in Fig. I-71 originate from background, most of which comes from multiply-scattered beam particles from the FMA beamline entrance or the beamstop in the first split-anode region. The events inside the windows of Figs. I-71a and I-71b are from residues. There are no events inside the window of Fig. I-71c. Further analysis reveals that the events inside the window of Fig. I-71d are due to background rather than evaporation residues. This will be discussed below, after a preliminary discussion of the background.

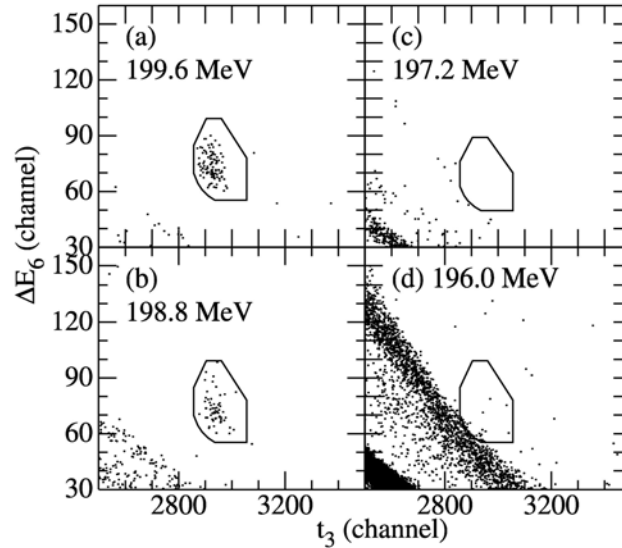


Fig. I-71. Two-dimensional plots of ΔE_6 versus t_3 obtained at incident energies of 199.6 MeV (a), 198.8 MeV (b), 197.2 MeV (c) and 196.0 MeV (d), respectively. The events inside the windows of (a) and (b) originate from evaporation residues. Other events are background.

The spectra in Figs. I-71a and I-71b represent about 5 and 12 hours of data, respectively, with an average beam current of 60 pA on target. The background is minimal. The m/q spectra in Figs. I-72b and I-72c were obtained by gating with a window around the respective residues in the ΔE_6 versus t_3 plots of Fig. I-71. Peaks at channels 103 and 146 are for $m = 162$ and $q = 23$ and 24, respectively. The m/q spectrum of Fig. I-72a, which was taken at a higher incident energy with larger cross sections, is included for comparison. The spectrum in Fig. I-71c represents 3 hours of data only, shorter than Fig. I-71b (12 hours), but the background is higher. Figure I-71d, a 15

hours run, exhibits even more intense background. The sources of this background are still uncertain. It is not simply proportional to the beam current or the integrated dose. The only differences between the data of Figs. I-71b, c and d are the beam energies and the E_0 setting of the FMA. The incident energies, E_{lab} , were 198.8, 197.2 and 196.0 MeV, and the FMA was set for $E_0 = 71.8$, 71.0 and 71.0 MeV, respectively. This means that small differences in these energies or slightly different beam-tuning settings resulted in scattering from more "sensitive" regions of the FMA. This background will be examined in more detail in future studies.

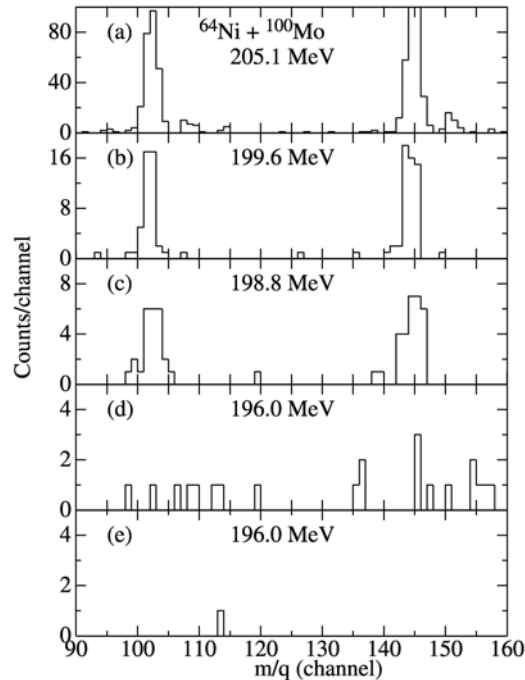


Fig. I-72. Position (m/q) spectra obtained at the various indicated energies of 205.1 MeV (a), 199.6 MeV (b), 198.8 MeV (c), 196.0 MeV (d) and 196.0 MeV (e), respectively. The events correspond to counts inside the respective windows of Fig. I-71, but for (e), the additional window (Fig. I-74) is applied as well. See text for details.

Despite the increased background of Figs. I-71c and I-71d, the residue separation is still rather clean. For both of these runs, a rather large window in the ΔE_6 versus t_3 spectrum was used. For clarity, Figs. I-71b and I-71d are reproduced in Fig. I-73, with open circles representing the events inside the windows. Each event inside the window was then fully tracked to check whether it corresponded to a real evaporation residue event or to a background event. For example, there are 23 events inside the window of expected residues in Fig. I-71d. Their respective m/q spectra are shown in Fig. I-72d. These 23 events are rather random in m/q , with residue-candidates around channel 103 and 146. Examining the plots of ΔE_5 versus t_3 shown in Fig. I-74b reveals that 22 of these 23 events fall outside the indicated window for

the location of the expected residues. Figure I-74a is the same ΔE_5 versus t_3 plot corresponding to the measurement of Fig. I-73a, where the open circles are residue events inside the ΔE_6 versus t_3 window. There is one event inside the expected window in Fig. I-73b. Its m/q value, shown in Fig. I-72e, lies outside the expected m/q peaks around channels 103 or 146. Even though several background events are located inside the ΔE_5 versus t_3 window in Fig. I-74a, they are outside the ΔE_6 versus t_3 window in Figs. I-73a or I-71b. Further checks utilizing all of the other signals and tracking methods mentioned above clearly reveal that for the last two energies, these "candidate" events were all associated with background. Hence, only upper limits for the measured cross sections could be determined.

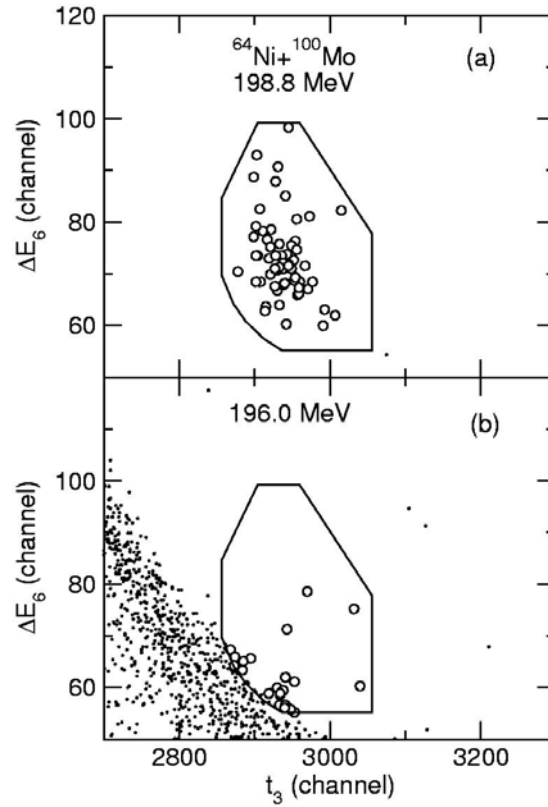


Fig. I-73. Enlarged views of Figs. I-71b and I-71d, respectively. The isolated group in (a) (open circles) originates from evaporation residues, whereas the other events are caused by background. At $E = 196.0 \text{ MeV}$ (b), 23 events (open circles) fall inside the acceptance window for evaporation residues. Further analysis (Figs. I-72 and I-74) shows that these events are background, as discussed in detail in the text.

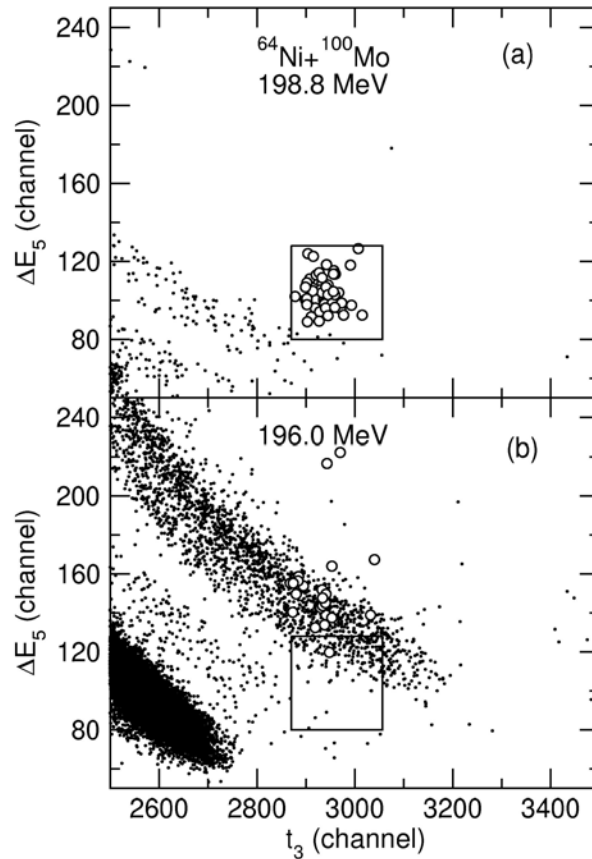


Fig. I-74. Two-dimensional plots of ΔE_5 vs. t_3 obtained at incident energies of 198.8 MeV (a) and 196.0 MeV (b). Open circles are the events inside the ΔE_6 versus t_3 windows in Figs. I-73a and I-73b, respectively. See text for details.

It was found that, with the upgraded FMA and the present detector system, a beam suppression factor of about 4×10^{-17} can be achieved for the Ni + Mo system. The experimental result for the $^{64}\text{Ni} + ^{100}\text{Mo}$ and other related details of the experiment can be found in Ref. 7.

Five main conclusions can be drawn from the present work are as follows: 1) Even for a rather low energy heavy-ion fusion experiment, full tracking of the evaporation residues is possible and important, especially for low cross section measurements where background suppression is crucial. For this purpose a new detector system has been built and successfully deployed. 2) For the new focal plane detector system of the FMA, the longer flight path and the ΔE signals near the end of the track give the most useful

information for the separation of residues from background. 3) A rather clean separation between evaporation residues and background events can be achieved by using a two-dimensional $\Delta E_6 - t_3$ spectrum, resulting in cross sections down to the ~ 300 nb level for the $^{64}\text{Ni} + ^{100}\text{Mo}$ system. For even lower incident energies, full tracking is necessary to identify the good events. The new detector system also avoids the detector damage problem frequently experienced with Si solid-state detectors at the FMA focal plane. 4) With the upgraded FMA and the new detector system, a beam suppression factor of about 4×10^{-17} has been demonstrated. 5) The sources of some of the background events are still unknown. The new detector system will allow us to study the background in more detail, thereby enabling the measurement of even smaller cross sections.

*University of Notre Dame, †Hebrew University, Jerusalem, Israel.

¹C. L. Jiang *et al.*, Phys. Rev. Lett. **89**, 052701 (2002).

²C. L. Jiang *et al.*, Phys. Rev. C **69**, 014604 (2004).

³C. L. Jiang *et al.*, Phys. Rev. Lett. **93**, 012701 (2004).

⁴D. G. Kovar, D. J. Henderson, and B. B. Back, ANL Phys. Div. Annual Report **ANL-90/18**, 108 (1990).

⁵T. O. Pennington *et al.*, ANL Phys. Div. Annual Report **ANL-03/23**, 105 (2003).

⁶A. N. James *et al.*, Nucl. Instrum. Methods **A267**, 144 (1988).

⁷C. L. Jiang *et al.*, Phys. Rev. C **71**, 044613 (2005).

h.6. Performance of a Compton Camera Using Digital Pulse Processing (C. J. Lister, E. F. Moore, F. G. Kondev,* B. Philips,† and E. Wulf†)

Position sensitive hyperpure germanium wafers have considerable potential in many areas of imaging as well as in nuclear physics research. We have been working on an LDRD project to construct a Compton Camera capable of seeking and imaging sensitive materials. The camera has position sensitivity on two levels, “strip level” using analog electronics gives position resolution of ± 2.5 mm and “digital interpolation” level of ~ 1 mm. During this year we set up a fully digital Compton Camera at the Naval Research Laboratory in Washington, DC, and made our first measurements. These results were reported and have been published in the IEEE proceedings

from the Rome conference on advanced imaging techniques.¹ Good 3-D information was obtained, using rise time information to establish the depth of each interaction, and induced signals on neighbor strips to improve lateral location.

We also have established a procedure for the loan of sensitive materials from within ANL to test our detector system. We arranged the loan of a set of plutonium foils and mounted them in GammSphere in order to establish methods for determining the provenance of the material. Analysis of these data is in progress (Fig. 1).

*Nuclear Engineering Division, Argonne National Laboratory, †Naval Research Lab, Washington, D.C.

¹E. A. Wulf, B. F. Philips, W. N. Johnson, J. D. Kurfess, E. I. Novikova, C. J. Lister, and F. G. Kondev, Proceedings of the IEEE Nuclear Science Symposium and Medical Imaging Conference (NSS/MIC), Rome, Italy, October 16-22, 2004, to be published (2005).

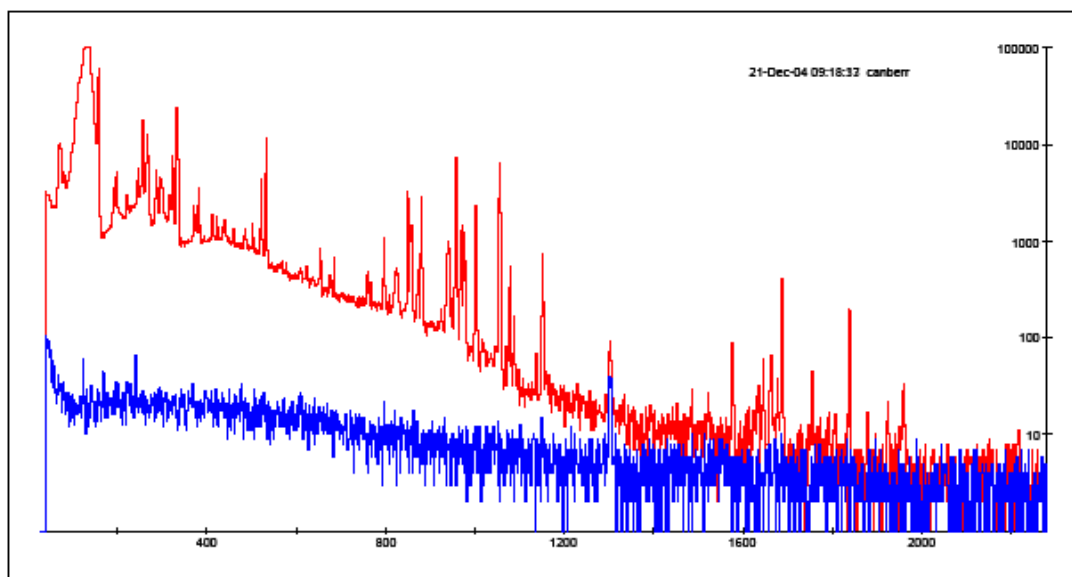


Fig. I-75. Gamma ray spectrum from a plutonium sample assayed with GammSphere. The intensity of various lines can be used to establish the exact isotopic makeup of the sample and hence its provenance.

h.7. Ambiguity in Gamma Ray Tracking of “Two Interaction” Events (N. J. Hammond, T. Duguet, and C. J. Lister)

Tracking of gamma-rays in germanium detectors can allow the full reconstruction of interactions, a feature that is useful in many applications. Scrutiny of the kinematics and geometry of gamma rays which are Compton scattered only once prior to full absorption reveals that there are special cases where even perfect spatial and energy resolution cannot resolve the true interaction sequence and consequently the gamma-ray tracks cannot be unambiguously reconstructed. The photon energy range where this ambiguity exists is from 255 keV to about 700 keV. This is an energy

region of importance for nuclear structure research and a domain where two-point interactions are probable.

We have made a careful analysis of this ambiguity and produced analytical formulae to identify the regions of difficulty. Figure I-76 shows an illustration of an event that cannot be properly reconstructed, even in a detector with perfect spatial and energy resolution. This research has been accepted for publication in *Nuclear Instruments and Methods*.¹

¹N. J. Hammond, T. Duguet, and C. J. Lister, *Nucl. Instrum. Methods* **A547**, 535-540 (2005).

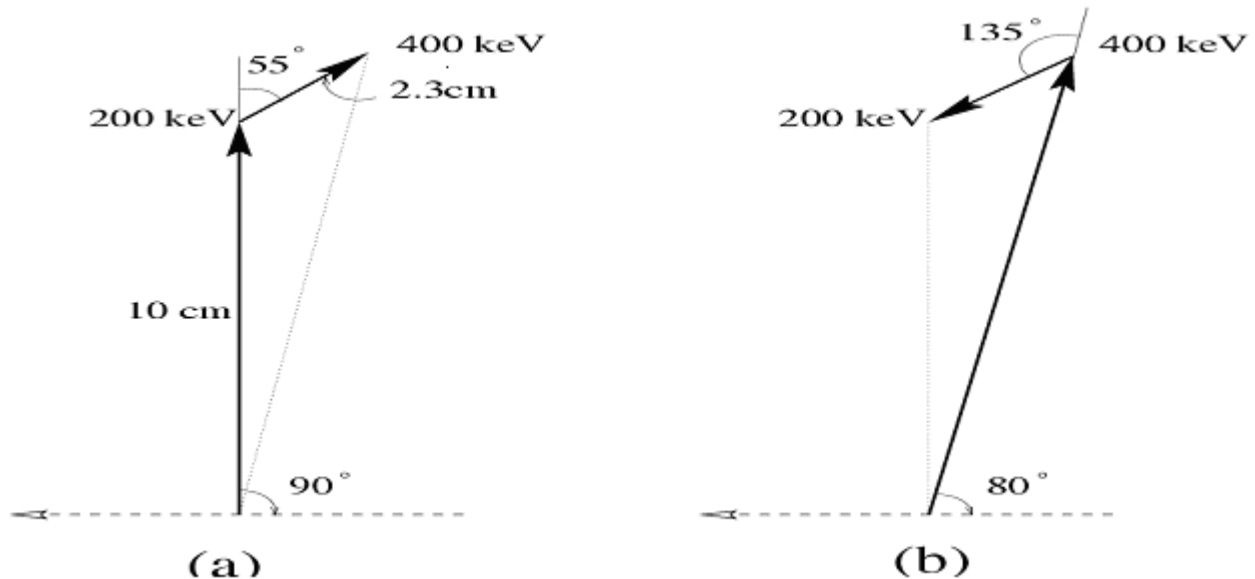


Fig. I-76. An example of an ambiguous event in which the energy deposition and the location of interaction points can be exchanged, so the true sequence of events is not resolvable.

h.8. A Bragg Scattering Method to Search for the Neutron Electric Dipole Moment

(M. Peshkin, G. R. Ringo, T. W. Dombeck,* D. S. Hussey,¶ D. L. Jacobson,¶ H. Kaiser,† D. D. Koetke,‡ T. D. S. Stanislaus,‡ R. K. Smither,§ and S. A. Werner¶)

The goal of this project is to measure the neutron EDM by observing the precession of the neutron spin in the crystalline electric field when the neutron undergoes several thousand Bragg reflections from a perfect silicon crystal. A preliminary experiment carried out at the Missouri University Research Reactor showed that the reflectivity coefficient of one of our crystals is greater than 0.9999, with 95%

confidence. In the past year we completed construction of a table to hold and orientate the crystal within the solenoid and we moved the experiment to the NIST reactor. Also, two NIST physicists, Daniel S. Hussey and David L. Jacobson, have joined the collaboration. In spring 2005, we will repeat the reflectivity measurement at NIST and plan to achieve an uncertainty in the reflectivity of 2×10^{-5} . The reflectivity measurement will

be followed in fall 2005 by a proof-of-principle experiment to measure the neutron's magnetic dipole

moment by the same method and in the same electric fields as in the EDM measurement.

*University of Hawaii, †University of Indiana, ‡Valparaiso University, §APS User Program, Argonne National Laboratory, ¶National Institute of Standards and Technology.

h.9. Heavy Element Scattering Chamber Upgrade (D. Peterson and J. Falout)

The heavy element scattering chamber¹ was designed to accommodate large-diameter rotating wheel targets necessary to withstand high beam currents. A recent experiment² performed at ATLAS required highly-enriched (>99%) ²⁰⁴Pb target material, the cost of which prohibited fabrication of a large target wheel. The chamber was therefore modified to accommodate a smaller target wheel designed for use with Gammasphere experiments since one could expect to produce two or three such wheels from a modest amount of target material. The primary modification required the translation of the rotation axis from the chamber center to only a few cm below the beam. Figure I-77 shows the solution. An aluminum mounting bracket attaches to the main shaft bearing housing via a C-clamp mechanism. A

wheel (below) directly mounted to the main axis drives the target wheel (top) with a nylon belt which is kept taut via an adjustable idler wheel assembly (left). The translation is a two-piece design so that the top wheel can be moved up or down relative to the bottom wheel in order to properly align with the beam axis. The idler shaft is also adjustable to maintain proper tension regardless of the spacing between the two main gears. The target wheel mounts directly to the top gear, which has openings to match the target frames. All gears are one-to-one, ensuring consistent rotational velocity relationships regardless of target wheel geometry. This assembly was successfully used in a 6-day run, rotating at velocities between 1100 and 1700 rpm with beam intensities up to 85 pnA. The Pb targets showed no effects of melting or unusual stress indicating the success of this design.

¹A. Heinz *et al.*, ANL 2001 Annual Report, ANL-02/15 (2002).

²D. Peterson *et al.*, section c.4. of this report.

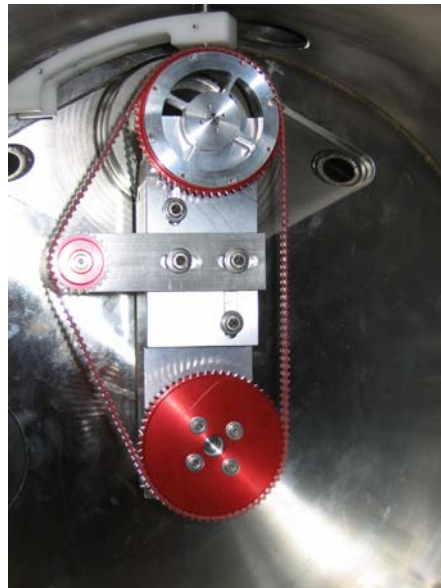


Fig. I-77. Photo of the new rotating target wheel assembly in place with a blank target wheel attached. See text for details.

h.10. The MUSIC Detector (B. Shumard)

A Multiple Sampling Ionization Chamber (MUSIC) was developed for use in conjunction with the ATLAS Scattering Chamber (ATSCAT). This chamber was developed to study the (α, p) reaction in stable and radioactive beams. We will use the counter gas of an ionization chamber as a target (either CH_4 for hydrogen) or He and detect both particles in the outgoing channel ($p + \text{beam particles}$ for elastic scattering or $p + \text{residual nucleus}$ for (α, p) reactions). The MUSIC detector will be followed by a Si detector to provide a trigger for anode events. The anode events will be gated by a gating grid so that only (α, p) reactions where the proton reaches the Si detector will show a signal on any one of the anode pads.

The MUSIC detector works as a segmented Ionization Chamber. The active area of the chamber is 11.95 in. and is divided into 16 equal anode segments (3.5 in. \times 0.70 in. with 0.3 in spacing between pads). The dead area of the chamber was reduced by the addition of a Delrin snout that extends 0.875 in. into the chamber from the front face. The snout is fitted with a reinforced mylar window capable of withstanding 300 torr of internal pressure. 0.5 in. above the anode is a Frisch Grid that is held at ground potential. 0.5 in. about the Frisch grid is a gating grid. The gating grid functions as a filter, stopping the drift of electrons to the anode,

effectively halting the gathering of signals. This is accomplished by setting two alternating sets of wires at differing potentials. This creates a lateral electric field which effectively traps the drift electrons rather than allowing them to pass on to the anode. The gate can be opened by removing the voltage gradient between the alternating wires (*i.e.* setting both sets of wires at equal potential). The chamber also has a reinforced mylar exit window which allows a Si detector to be placed at the end of the chamber in vacuum. This allows for protons from the (α, p) reaction to be detected. The detection of those protons will trigger the gating grid to the open state to allow the drift electrons released from the ionizing gas during the (α, p) reaction to reach the anode segment below the reaction. The segmentation of the anode allows a reaction vertex to be determined. Figure I-78 shows a photograph of the detector.

In a first test we plan to measure the use of the MUSIC for a measurement of elastic proton scattering on ^{10}B at an incident energy of 3 MeV/u. We then plan to bring the incident energy up to 6 MeV/u and proceed to a measurement of the $^{10}\text{B}(p, \alpha)^7\text{Be}$ reaction. The high energy branch of the alpha's ($E > 40 \text{ MeV}$) will be a clear signature for a (p, α) reaction. (To stop all the recoiled ^7Be within MUSIC, we have to scarifify the low energy alpha branch.). In a third run, we then plan to bring the energy down to 3.0 MeV/u again to study the $^{10}\text{B}(\alpha, p)^{13}\text{N}$ reaction by adding ^4He to the counter gas.

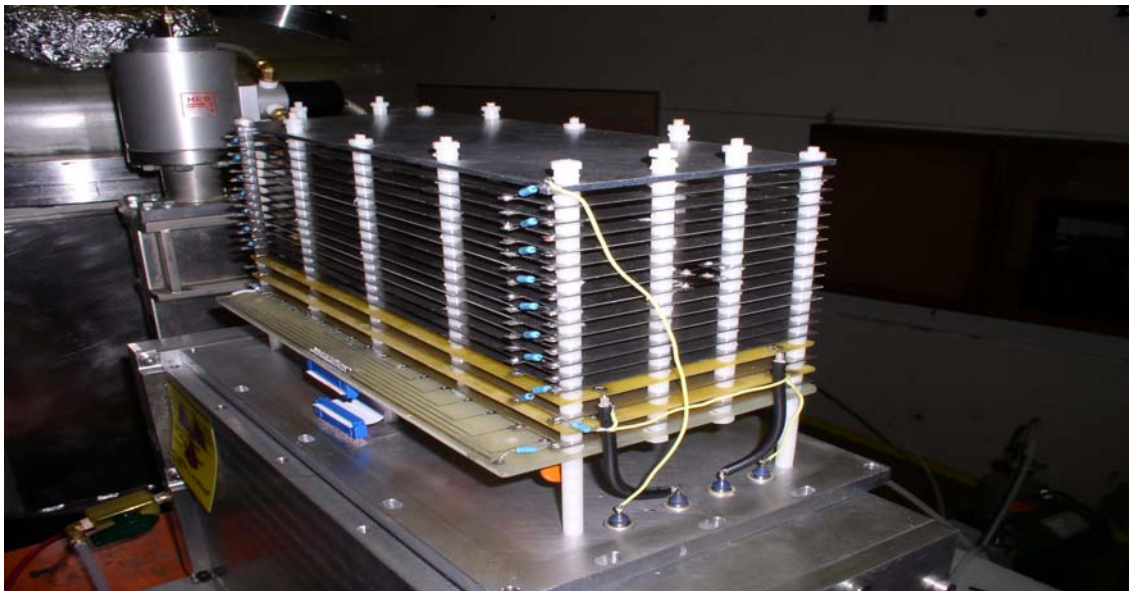


Fig. I-78. The Multiple Sampling Ionization Chamber. The photograph is of the electrode structure of the detector standing on top of the vacuum chamber in which it operates.

h.11. Digital Bragg Curve Spectroscopy (X. Tang, K. E. Rehm, and R. C. Pardo)

Digital Signal Processing (DSP) has been widely used in many aspects of nuclear physics. The detail information from the detectors, captured by a high-speed waveform recorder, provides more possibilities and flexibilities to the nuclear physicists compared to traditional analog modules. In the past year, we studied the waveforms captured from our Bragg detector,¹ located at the focal plane of the Enge spectrograph, with a mixed ^{12}C , ^{15}N , ^{18}O beam with an energy of 40 for ^{12}C , 50 MeV for ^{15}N and 60 MeV for ^{18}O . The signal from the charge sensitive pre-amplifier was feed into a wide-band amplifier (Phillips 778) to match the input range of the digitizer. The amplified signal is then digitized with a LR2262 waveform recorder. The waveform recorder was working in post-trigger mode with a trigger coming from the PPAC detector. The signal

was sampling at a speed of 80 MHz with a resolution of 1024 bits. The digitized spectrum after a triangle filter is shown in Fig. I-79. In this figure, ^{12}C , ^{15}N , ^{18}O , ^{24}Mg and ^{27}Al are clearly identified without the use of any algorithm. Meanwhile, the signal was also feed into analog modules for comparison. The energy from the DSP is obtained with a trapezoid filter.² The range is measured by the timing between the PPAC and the Leading Edge Discriminator (red line in Fig. I-79). The results from digital signal processing are comparable with those from analog signal processing. To demonstrate the advantage of DSP, we will try to identify some heavier isotopes, which are difficult to resolve for analog technique. The authors would like to thank I.-Y. Lee of LBNL for providing DSP programs and encouraging discussions.

¹K. E. Rehm and F. L. H. Wolfs, Nucl. Instrum. Methods **A273**, 262 (1988).

²V. T. Jordanov and G. F. Knoll, Nucl. Instrum. Methods **A345**, 337 (1994).

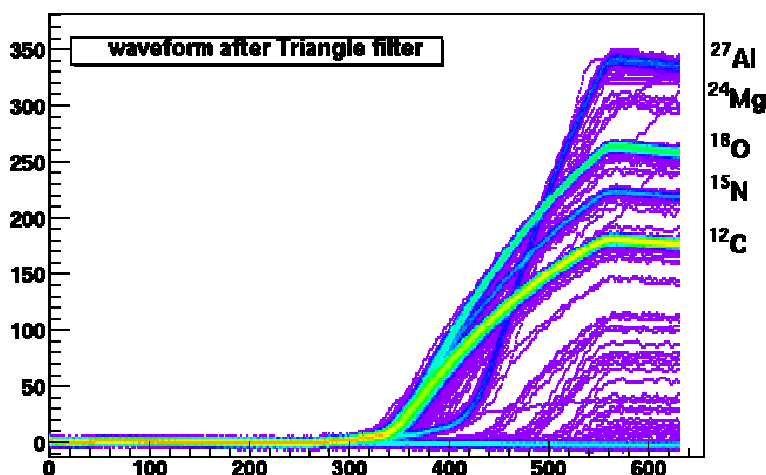


Fig. I-79. The digitized signal from the charge-sensitive preamplifier. The ^{12}C , ^{15}N , ^{18}O , ^{24}Mg and ^{27}Al are clearly separated.

h.12. The New Focal Plane Detector for the Notre Dame Spectrometer (P. Collon)

The study of reactions induced by stable and radioactive beams requires powerful detection techniques. One of these techniques is the use of a magnetic field to separate the reaction products from the initial beam as well as any beam-induced background. We are currently developing the gas-filled magnet isobar separation technique using the Brown-Buechner vertical spectrograph at the Nuclear

Structure Laboratory of the University of Notre Dame. The interest for having a gas-filled magnet both for Accelerator Mass Spectrometry (AMS) as well as for the study of nuclear reactions with low cross sections stems from its basic property of physically separating the trajectories of ions of different elements. This is of particular interest for nuclear astrophysics where the identification of specific reaction products requires their

separation from other interfering reactions as well as machine background that are often several orders of magnitude higher in intensity than the isotope of interest. This technique has already successfully been applied to the detection of such isotopes as ^{39}Ar , ^{44}Ti , ^{63}Ni and ^{182}Hf .

The ND Brown-Buechner spectrograph is currently being upgraded with new vacuum control and pumping systems, new LabView controls, beam optics and in particular a new focal plane detector. The original photo-plate detection system at the focal plane is being replaced by a new multi-wire position sensitive proportional counter and ionization chamber that was built with the help of a Notre Dame undergraduate student (S. Kurtz) in collaboration with Argonne National Laboratory (D. Henderson and B. Shumard). This detector with an active window of 470×114 mm will also be fitted with an ionization chamber following the position sensitive

counter (see Figs. I-80a and I-80b). Both chambers of the detector have independent gas handling systems that were developed in parallel to the detectors. Thin mylar windows ($350 \mu\text{g}/\text{cm}^2$) will both provide the entrance windows and enable to run both chambers at independent pressures while providing minimal energy loss for the particles. This project, which started in the Summer of 2004 and has been running through 2004 and 2005 provided an incredible research and development opportunity for a Notre Dame undergraduate student by giving him the possibility of working with experts in the field of gas filled detectors from Argonne National Laboratory during his undergraduate time, as well as providing the Nuclear Structure Laboratory with fantastic technical support for the construction of a new detector that will be used for highly sensitive and cutting edge measurements in the field of nuclear astrophysics. Continual support during the year has made it possible to test and calibrate the system with maximum efficiency.

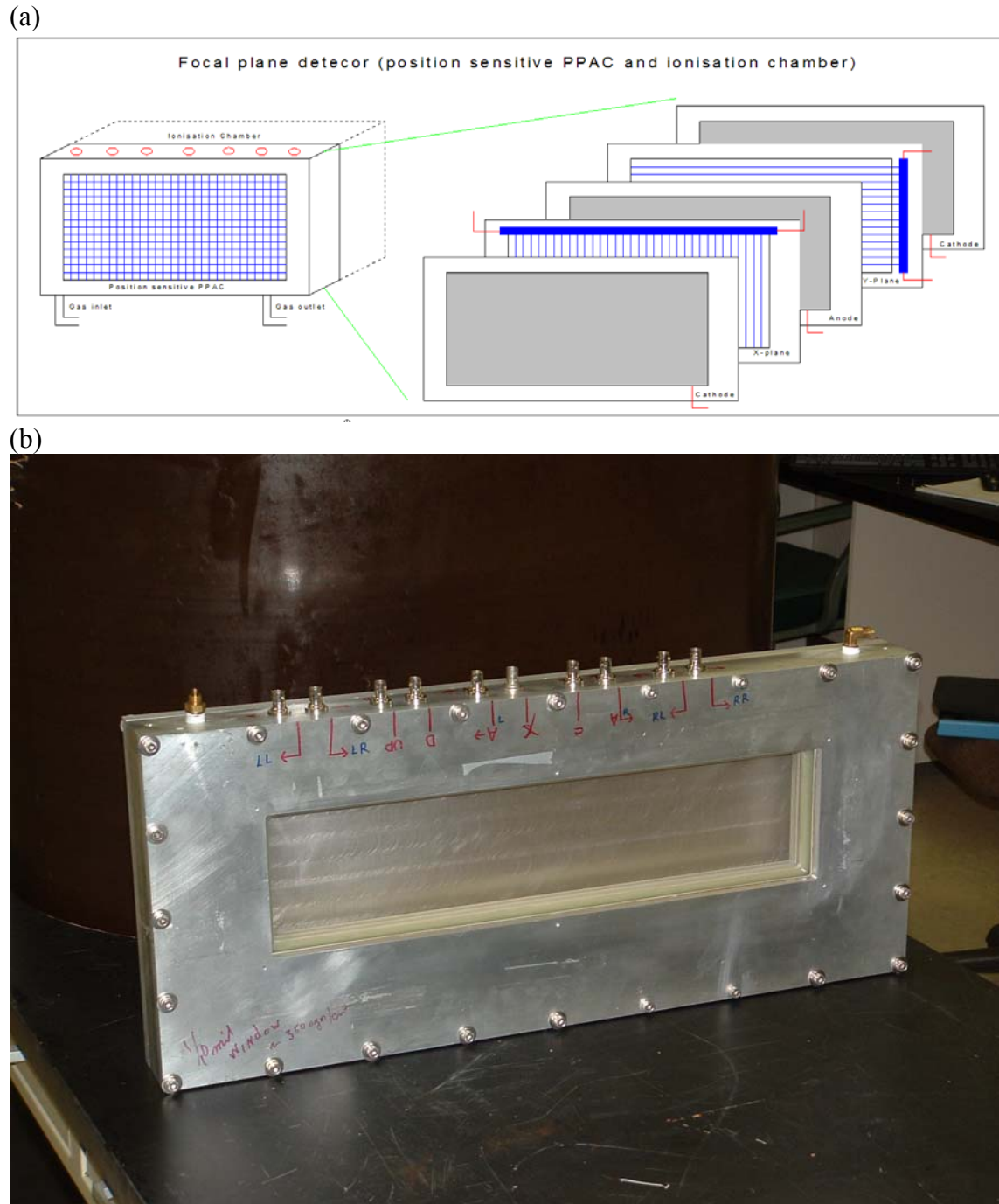


Fig. I-80. (a) illustrates the different planes of the position sensitive proportional counter that will constitute the front part of the new ND focal plane detector. (b) A picture of the actual detector. The active window is 470×114 mm.

h.13. Deployment of a Centrally Managed Windows Cluster (C. Stuart)

Within the past year the Division's Windows infrastructure has undergone many changes.

Originally, the system management was decentralized and the PCs were intermittently updated for cybersecurity.

All desktop computers were standalone. There was no easy way of sharing data. There were very few shared resources available to users who had Windows desktops.

Today, all systems are members of a centralized Windows domain (about 140 desktops). There are many resources and benefits available now that were not in the past. Everyone can now use a single username and password to access systems and resources. Before, everyone had to have a different username and password. There are now many network resources available. There is now a central file server. Users can now store their data on the server and access it from anywhere, on and off-site. This makes sharing data between colleagues a lot easier. There is a central print server. Users connect to printers through this server. Any changes, or updates, made to the printer settings are automatically set for everyone connected. There is a

new e-mail solution, as well. It has a very intuitive web interface as well as a slew of very useful features, such as online calendaring and a Global Address List which contains all of the contact information for everyone working at the Laboratory.

This centralization of resources has also improved the Division's security stance. There is now a centralized antivirus service which forces updates down to the clients. There is now a two-front patch management system forcing updates to each of the clients. By improving the security of the systems we can more confidently guarantee the integrity of our data.

Each server is backed up regularly. If a user accidentally deletes a file from the file server, it can be restored. Just as important, if a server fails, it can be restored in a minimal amount of time. Migrating all the users to the new e-mail system is in progress.

h.14. Status of the SCARLET Data Acquisition System (K. Teh)

There are presently four single-CAMAC-crate SCARLET systems that have been assembled and deployed. One system has been used for "online" experiments at the FMA and the Enge Spectrograph. A second system is located at the Argonne Penning Trap. The third system is used for "offline" development of the Germanium strip detectors while the most recent system is used by members of the Chemistry Division at the APS.

All of the systems use a commercial Wiener CC32 CAMAC-PCI interface for crate control. A programmable CAEN interface takes the experimenters event trigger and initiates readout, and also returns an "end-of-event" signal for generation of a "readout-busy" signal. The acquisition systems comprises of two rack-mounted PCs, one to drive the CAMAC interface (ROC1) and one to build events and deliver them to the ethernet link. One (or more) further PCs can be used to control the acquisition, archive the data to disk, and visualize the data, using the CERN "Root" sorting package. Progress towards a multi-crate system has been slow, with several options being explored, but each showing shortcomings. It is hoped that a commercial module can be found that

will offer a simple and cost-effective solution to trigger and busy legislation and keeping the data from multiple crates synchronized.

A new data acquisition infrastructure will be set up this year to fully support the SCARLET deployments. Issues of the architecture of this infrastructure were discussed at length with staff scientists and representatives from the ATLAS Users Group. It was decided that the infrastructure should include a "farm" of computers for data analysis, a large disk array to store data, and an assortment of tape drives. An earlier idea to support remote retrieval of data via anonymous FTP was deemed inadvisable and has been shelved for the moment. The hardware for the analysis farm and the disk array have been procured and work is underway to set them up. Finally, work is also underway to develop monitoring software based on CERN's ROOT system. It was decided that the ROOT system, while extremely powerful and flexible, was too unwieldy for the kinds of data analyses performed at ATLAS. A plan to develop a more specific DAPHNE-like interface to ROOT was discussed and it is expected this software will be deployed together with the new infrastructure in the data room.

h.15. Progress on the New Gammasphere Data Acquisition (T. Lauritsen)

The commissioning of the new Gammasphere Data acquisition (DAQ), which was built at LBNL, has continued. This new DAQ will replace the old DAQ with the Motorola "event filter formatters" (EFFs). Among other things, a 'watchdog' function was implemented that monitors various errors in the data assembled by the eventbuilder VME module. If this monitor senses that the eventbuilder is producing invalid data, it will reset the eventbuilder. Thus, the DAQ will now recover and the DAQ will continue after a momentary interruption. Such a function is also necessary in the current DAQ. Numerous other functions needed to control the new DAQ have been

implemented as well. A thorough documentation of the new DAQ has been written and placed on the WWW along with the current "online" documentation for Gammasphere.

The new DAQ now appears quite stable, running for days with just sources in the array. On two occasions the new DAQ has been used "online" for short periods with in-beam data. In both cases the DAQ performed well. More tests will be performed during a variety of upcoming experiments, to thoroughly test the new DAQ before it is deployed. The infrastructure for writing all the data to disk, as opposed to tape, is being developed.

h.16. Gammasphere Operations (M. P. Carpenter, C. J. Lister, R. V. F. Janssens, T. L. Khoo, T. Lauritsen, J. Rohrer, E. F. Moore, D. Seweryniak, P. Wilt, S. Zhu, P. Chowdhury,* and F. G. Kondev†)

In the fall of 2002, Gammasphere was successfully relocated from Berkeley National Laboratory to the ATLAS facility at Argonne. All Ge detectors were annealed and all BGO bases repaired. Gammasphere was reassembled in area IV on the FMA beamline during January 2003.

In 2004, twenty-one PAC approved experiments were completed using Gammasphere. This can be compared to thirty experiments performed the previous year. The decrease in the number of experiments can be attributed to (i) the move of Gammasphere from the FMA beamline to the stand alone beamline and (ii) a decrease from 7-day operations to 5-day operations at ATLAS. With regards to the move of Gammasphere, the device was out of operations for two and half months.

By the end of 2004, Gammasphere had been operating at ATLAS for nearly two years, and it appears that the device will operate at our facility for the foreseeable future. In 1997, 2000 and 2002, Gammasphere was moved after approximately two years of operation at the host facility. In each instance, all Ge detectors were annealed and optimum energy resolution was restored to the array. Since Gammasphere is not scheduled to move from

Argonne, we have undertaken a policy to anneal a detector once its resolution has degraded beyond 3 keV at 1.33 MeV. As a result, we are annealing on average five detectors a month, and we anticipate this number to stay constant in the future. The three new Ge detectors ordered from ORTEC have been delivered. Two were accepted and are operating in Gammasphere. The third was returned to the vender to fix a mechanical problem.

As reported in the last annual report, due to failures of the resistors along the bias chain, we continue to see breakdowns on the BGO PMT bases. This results in a non-responsive channel. The PMT can be repaired by locating the failed resistor and replacing it, however, this is a very time consuming operation. While it is our plan to replace all of these bases with new components in the long run, we still are repairing the bases as they fail and as the schedule allows.

Several upgrade paths are being pursued. A replacement for the dual crate VME acquisition system has been developed and debugged. VME readout capabilities are finalized and in the testing stage. Finally, a move of Gammasphere from the FMA beamline to the old APEX beamline occurred in May, 2004. Details of the move can be found in separate contribution to the annual report.

*University of Massachusetts-Lowell, †Nuclear Engineering Division, Argonne National Laboratory.

h.17. Gammasphere Move (C. J. Lister, M. P. Carpenter, R. V. F. Janssens, T. Lauritsen, J. Rohrer, B. Zabransky, B. Nardi, P. Wilt, S. Zhu, and P. Chowdhury*)

To maximize the physics potential of both Gammasphere and the FMA, we have made Gammasphere “portable” allowing it to operate with the FMA (as it did during the 1997-2000 campaign), or in “standalone” mode (as it was operated during the 1995-1997 and 2000-2002 Berkeley campaigns). Preparation for the move was performed in 2003 and moving Gammasphere was performed for the first time in 2004. The new location of Gammasphere is about 4 meters from the FMA at the former APEX beamline.

Before the move could take place, many issues needed to be resolved. We investigated movement by crane, airpads and rollers. Rollers were finally selected on the grounds of cost. The floor and trench areas needed stiffening to permit the move of the device. A test move of the Gammasphere platform was successfully conducted using a test load of 15 tons of shielding blocks in 2003. Detailed plans for the re-routing of LN₂ and signal cables were also completed in 2003.

The move itself was done in June of 2004. The biggest challenge was the maintenance of the signal infrastructure. The detectors need to be kept cold and the amount of time the detectors are not-biased

minimized. Both requirements were necessary in order to prevent a need to disassemble the array and anneal all 101 Ge detectors. This also demands that the physical transition must be completed in less than 8 hours.

The move was carried out in May 2004. First, all the grey cables were disconnected and taken down from the cable trays and the LN fill system disconnected. The Gammasphere frame was then jacked up and placed on the rollers. Finally the device was slowly rolled from the FMA beamline to the new beamline. Approximately fifteen people assisted in pushing and pulling Gammasphere across the floor and the whole process took half a day. The grey cables and LN system were then reconnected before the next scheduled fill sequence, thus completing the move in under 8 hours. After bias was reapplied to the Ge detectors, no appreciable degradation in energy resolution was observed and the move was deemed a success.

While the physical move of Gammasphere took only a day, pre-move preparation and permanent installation afterwards requires significant effort, in excess of 1 FTE. As a result, we do not anticipate moving the device more than once a year. The move back to the FMA is scheduled for late 2005, approximately 18 months after the initial move.

*Sabbatical visitor from the University of Massachusetts-Lowell.

h.18. X-Array Developments (C. J. Lister, T. L. Khoo, R. V. F. Janssens, M. P. Carpenter, and S. Zhu)

The X-Array is designed to enhance gamma ray detection for many kinds of offline spectroscopy, such as α - γ , p - γ , β - γ coincidences, or isomer decays, that may be measured at the FMA focal plane or at the open geometry APT. The concept is to construct a flexible and compact box detector with modest segmentation but very high efficiency. We have procured three large “clover” detectors that are now frequently used in a variety of experiments, most significantly in a campaign at the FMA focal plane (Fig. I-81) which were critical in investigating isomers in ²⁵⁴No (for example, see section c.7. in this report). Further procurement of two more large clover detectors, to complete the box, has been delayed by the sharp rise in the Euro/Dollar exchange rate.

An opportunity for significant enhancement of our offline system has come from a decommissioned gamma-array owned by the DOE remote sensing laboratory. Fourteen large (100% relative efficiency) germanium crystals were transferred to ANL under an agreement that called for refurbishment, followed by a long-term loan for research. The refurbishment called for remounting the crystals in liquid nitrogen cooled cryostats. These counters will enhance our capabilities for “offline” counting and will be used in the X-Array. Figure I-82 shows some of the detectors delivered to ANL with their “Joule-Thompson” cooling system, prior to return to ORTEC for refurbishment.

The construction of a new FMA focal plane vacuum envelope has been hampered by shortage of resources. A

cost-effective partial rebuild of the chamber to allow the mounting of three clover elements (Fig. I-81) was implemented, which has provided much useful guidance for the full rebuild. In the light of this experience, the design of the new focal plane is being revisited, and construction should be finished in calendar year 2005.

To date, the electronics we have used for the X-Array have been culled from the former ANL-ND BGO Array. This has been quite successful, but many modules are >20 years old, and shown some unreliability, so some refurbishment with more modern modules is needed for optimum use. A dedicated setup is being established to facilitate use of the array. This investment will start in calendar year 2005.

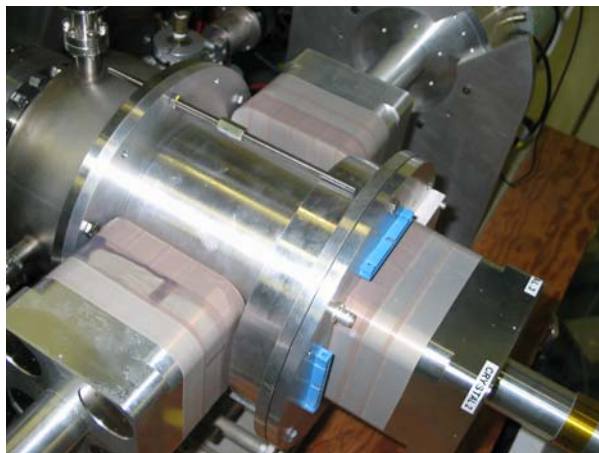


Fig. I-81. The three clover arrangement used in the spectroscopy of ^{254}No isomers. The mass-separated residues arrive across the FMA focal plane (top left) and are implanted in a silicon DSSD mounted at the center of the cylindrical spool. Gamma rays are detected in a clover detector mounted behind the DSSD (bottom right), and two further counters mounted on either side of the chamber.



Fig. I-82. Six of the large germanium detectors obtained from the DOE Remote Sensing Laboratory for refurbishment. The crystals are being remounted in liquid-nitrogen cooled cryostats for laboratory use.

h.19. Degradation of the ^{16}N Beam to Very Low Energy (M. Notani, R. C. Pardo, K. E. Rehm, X. D. Tang, J. P. Greene, A. Hecht, D. Henderson, R. V. F. Janssens, C. L. Jiang, E. F. Moore, J. P. Schiffer, S. Sinha, M. Paul,* R. E. Segel,† L. Jisonna,‡ and A. Wuosmaa‡)

In the ANL experiment, the ^{16}N beam is produced by bombarding a deuterium-filled cryogenic gas cell with a 82 MeV beam of ^{15}N . $^{16}\text{N}^{7+}$ ions produced via the $d(^{15}\text{N}, ^{16}\text{N})p$ reaction are then focused with a superconducting solenoid, located immediately behind the production cell, and are subsequently separated from the primary beam with a 22° bending magnet. A superconducting debunching resonator

improved the energy width of the secondary beam to about 61.3 ± 0.3 MeV. The secondary particles were identified with respect to mass and Z in the focal plane of the split pole spectrograph. Figure I-83 shows a plot of particle range vs. energy indicating the purity (80%) and the observed beam contaminants. All of the contaminants are stable isotopes and, therefore, do not result in any heavy-ion – alpha coincidences.

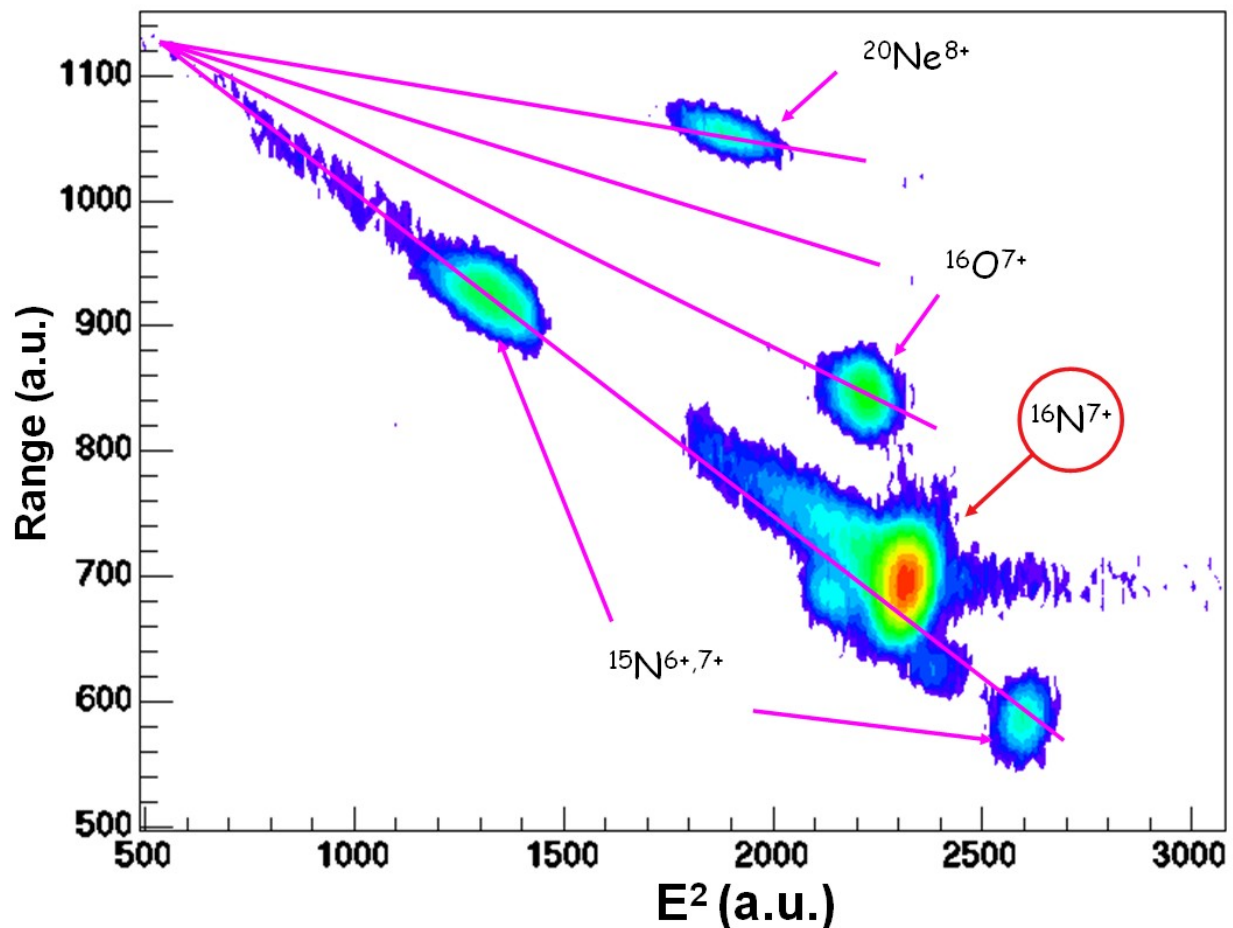


Fig. I-83. Particle identification spectrum measured in the focal plane of the magnetic spectrograph. The various particle groups are identified in the figure.

The 60 MeV ^{16}N ions are first slowed down in the 16-cm long attenuation cell filled with P10 gas, with 1.3 mg/cm^2 thick Ti foils as entrance and exit windows. An additional Al absorber, installed after the attenuation cell, reduces the energy of ^{16}N ions to about 250 keV. The Al absorber replaced a similar Mylar foil, which in an earlier test experiment was

damaged when it was hit by an intense ^{15}N beam during the beam tuning procedure. The gas pressure in the attenuation cell can be adjusted independent of the pressure in the ionization chamber volume, in order to maximize the number of ^{16}N particles stopped in the $10 \text{ }\mu\text{g/cm}^2$ thick carbon catcher foils (see Fig. I-84a).

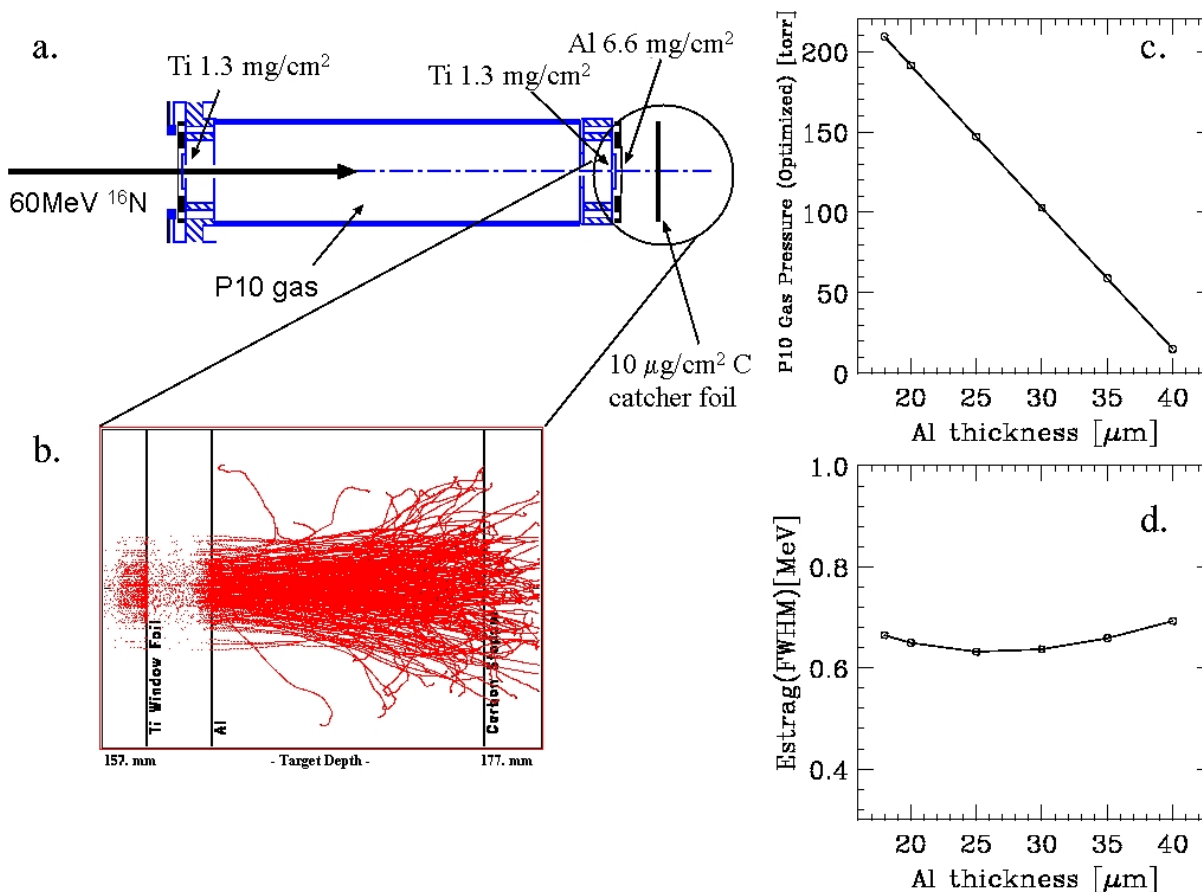


Fig. I-84. (a) Layout of the experimental setup to attenuate the ^{16}N particles for measuring the beta-delayed alpha decay of ^{16}N ; (b) Particle trajectories of ^{16}N calculated with the program SRIM¹ in the vicinity of the carbon stopping foil; (c) Gas pressure (P10) in the attenuation cell needed to stop the ^{16}N particles in the carbon catcher foil as function of the Al absorber thickness; (d) Energy spread of ^{16}N particles at the C catcher foil as function of the Al absorber thickness.

The thickness of the Al absorber and the pressure in the attenuation cell were chosen to minimize the energy straggling of the ^{16}N beam at the catcher foil location. In Fig. I-84d, the calculated energy spread of the ^{16}N at the foil is shown as a function of the Al absorber thickness. Figure I-84c shows the P10 gas pressure needed to stop the ^{16}N particles in the C foil as a function of the Al thickness. Based on these simulations a 25 μm thick Al absorber was chosen for the experiment. Figure I-84b shows the results of a

TRIM calculation of the particle trajectories in the vicinity of the carbon stopping foil.

To determine the optimum pressure in the attenuation cell the percentage of ^{16}N particles stopped in the C catcher was measured with a Si surface barrier detector. The results are shown in Fig. I-85. The optimized pressure was found to be 146 Torr, in very good agreement with the calculated values. At the optimum pressure 5.5% of the ^{16}N were stopped in the foil.

*Hebrew University, Jerusalem, Israel, †Northwestern University, ‡Western Michigan University.

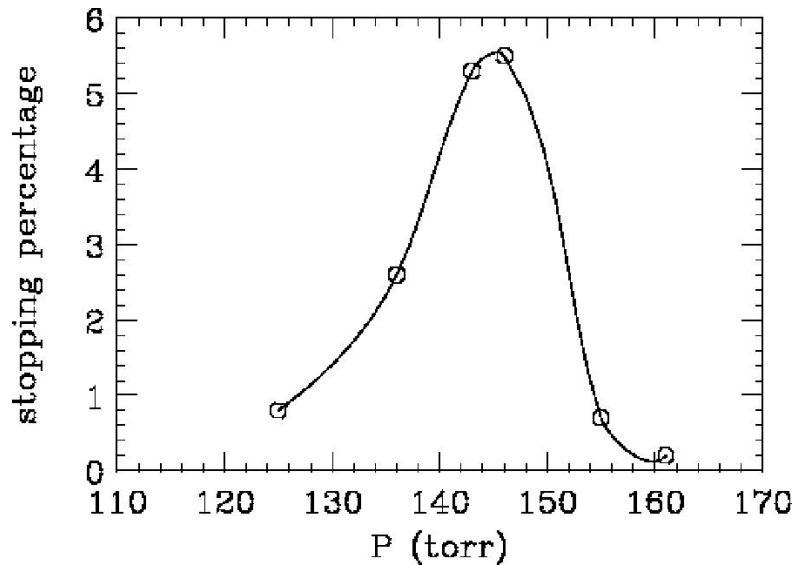


Fig. I-85. Measured stopping percentage of ^{16}N particles at the C catcher as a function of P10 pressure in the attenuation cell.

h.20. Improvement of the Experimental Setup for the Study of the ^{16}N β Delayed α Decay (B. Zabransky, B. Nardi, S. Gerbick, X. D. Tang, K. E. Rehm, and J. P. Schiffer)

For the measurement of the beta-delayed α decay of ^{16}N , a dedicated vacuum chamber containing two pairs of ionization chambers has been developed. Details are given in previous annual reports. In this reporting period, two major modifications have been implemented. The need to detect particles with very low energies (~ 100 keV) forced us to eliminate all possible sources of electronic interference. One of them originates from the stepping motor, which rotates the target wheel by 120° within 60 ms from the irradiation position into one pair of the twin ionization chambers. While the irradiated foil is being counted, the stepping motor keeps the sample in place using a small pulsed holding current. This current was found to induce a noise signal in the

amplifiers. To eliminate this interference, a mechanical brake was installed, which was activated once the wheel was in its proper position. With this brake the stepping motor could be switched off completely during the counting period.

The shape of the ^{16}N spectra was sensitive to the detailed geometry around the beam spot. ^{12}C or alpha particles emitted close to the plane of the foil and stopped in the target frame or the holding screws, produced signals that could distort a critical part of the spectrum. To eliminate these effects, larger asymmetric frames were designed with all crews located outside the ionization chamber. The geometry was optimized based on simulations that are described in section h.22.

h.21. The Twin Ionization Chambers (X. D. Tang, D. Henderson, K. E. Rehm, I. Ahmad, J. P. Greene, A. Hecht, R. V. F. Janssens, C. L. Jiang, E. F. Moore, M. Notani, R. C. Pardo, G. Savard, J. P. Schiffer, S. Sinha, M. Paul,* L. Jisonna,† R. E. Segel,† A. Champagne,‡ and A. Wuosmaa§)

Ionization chambers have several advantages over Si detectors for the measurement of the beta-delayed alpha decay of ^{16}N :

- Beta particles experience a very small energy loss (~ 3 keV in this experiment),
- They can be built with very high acceptances,
- They can be built with the required thickness and are very homogenous,
- They don't have any dead-layers,
- They don't experience radiation damage in long experiments.

For our measurement of the beta-delayed α decay of ^{16}N , we have built two pairs of gridded ionization chambers for the detection of α - ^{12}C coincidences.¹

Figure I-86 shows a photograph of the full setup. The two ion chambers (diameter 10 cm, depth 6.5 cm) share a common cathode, which also acts as a target wheel. The ionization chambers provide the standard energy signal from the anodes, and, in addition, information about the angle of emission with respect to the plane of the cathode, from the Frisch grids. The ionization chambers have been tested and calibrated with α sources (^{228}Th and ^{148}Gd) as well as with α - ^7Li coincidences obtained from the $^{10}\text{B}(n,\alpha)^7\text{Li}$ reaction using a PuBe neutron source. The neutron source was located outside the ionization chamber and two ^{10}B foils ($10 \mu\text{g}/\text{cm}^2$ evaporated on $10 \mu\text{g}/\text{cm}^2$ C) were mounted on the target wheel. The neutrons were thermalized in a 5 cm thick layer of high-density polyethylene.

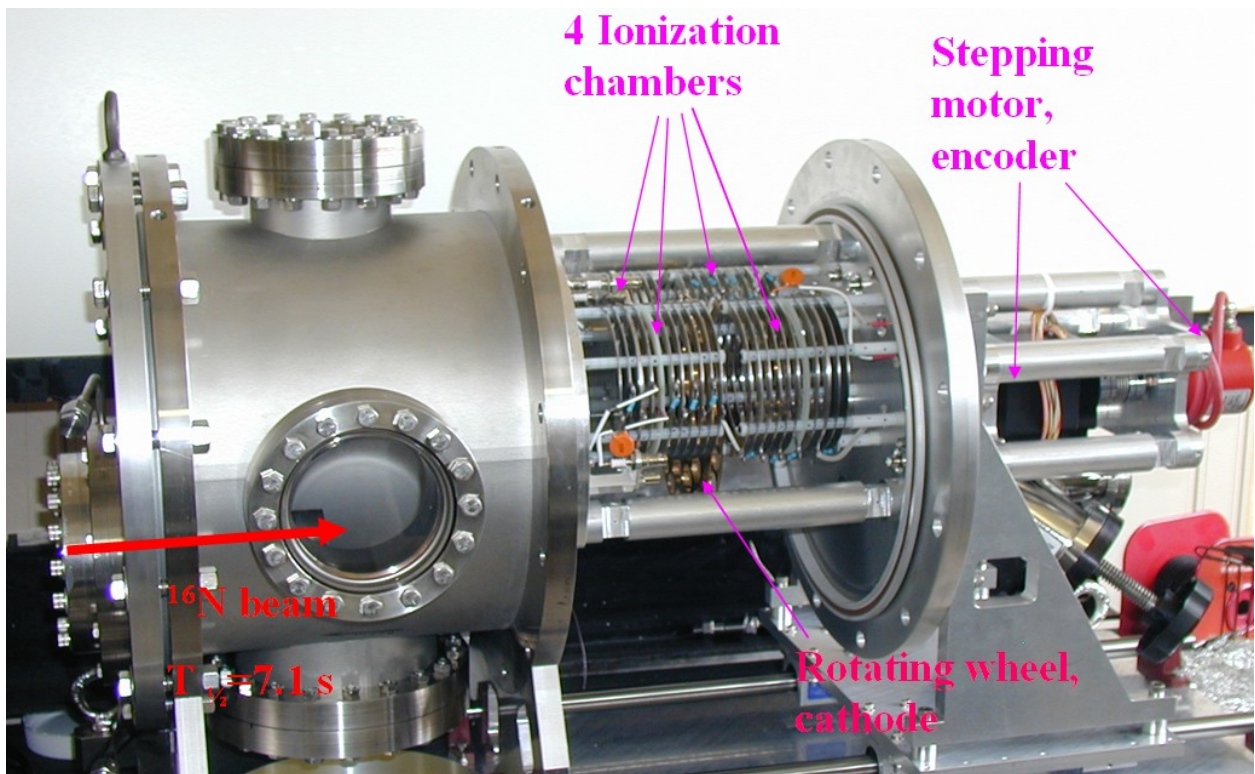


Fig. I-86. Photograph of the experimental setup for measuring the beta-delayed alpha decay of ^{16}N .

Alpha particles emitted perpendicular to the cathode produce a small signal on the Frisch grid, while alphas emitted along the foil's surface result in a

larger grid signal. A two-dimensional spectrum of grid vs. anode signal is given in Fig. I-87. The two vertical lines are due to the 1.483 and 1.789 MeV alpha particles,

produced in the $^{10}\text{B}(n,\alpha)^7\text{Li}$ reaction and emitted at different angles with respect to the foil, while the two lower-energy groups are caused by the coincident ^7Li particles, which have a smaller range in the ion chamber and are all stopped in the vicinity of the

target wheel. The energy resolution obtained from the 1.485 MeV line is 40 keV, sufficient to notice the difference in the energies of the alphas passing through the carbon backing.

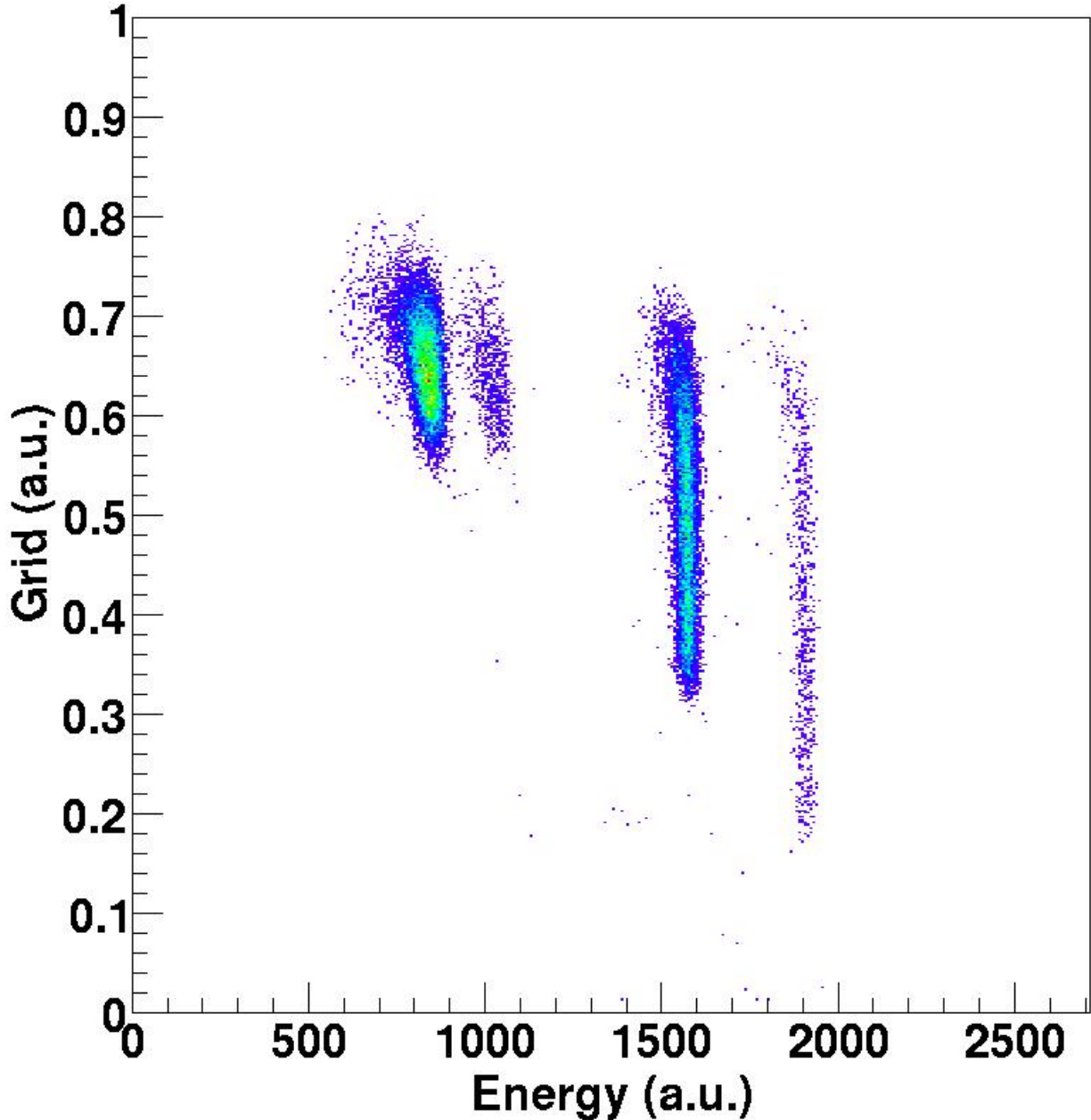


Fig. I-87. Spectrum of grid vs. anode signals measured in one of the twin-ionization chambers for ^7Li -alpha coincidences obtained from the $^{10}\text{B}(n,\alpha)^7\text{Li}$ reaction.

In order to use the kinematically calculated alpha energies one has to make sure that the reaction is induced by thermal neutrons. This was shown by repeating the measurement with an additional 1 mm thick Cd foil positioned behind the polyethylene. Under this condition the α - ^7Li coincidence rate is

reduced by more than a factor of 15, very close to the calculated value.

The stability of the detectors was measured over a period of 10 days. For three of the detectors, the stability was found to be better than 3×10^{-3} , while the fourth detector

showed a (temperature dependent) drift of about 40 keV. The electronics for this branch will be replaced. Altogether, the detector system proved to

be well suited for the new measurement of the beta-delayed α decay of ^{16}N .

*Hebrew University, Jerusalem, Israel, †Northwestern University, ‡University of North Carolina, §Western Michigan University.

¹C. Budtz-Jorgenson *et al.*, Nucl. Instrum. Methods **A258**, 209 (1987).

h.22. Backgrounds and Sensitivity to Beta Particles (X. D. Tang, M. Notani, K. E. Rehm, I. Ahmad, J. Greene, A. Hecht, D. Henderson, R. V. F. Janssens, C. L. Jiang, E. F. Moore, R. C. Pardo, G. Savard, J. P. Schiffer, S. Sinha, M. Paul,* L. Jisonna,† R. E. Segel,† A. Champagne,‡ and A. Wuosmaa§)

Because of the low count rates expected for the so-called interference peak in the ^{12}C - α coincidences in (typically 3 events/hour) the background in the twin-ionization chamber needs to be well understood. This was tested in a series of "offline" tests. In order

to stop α particles up to about 5 MeV, the pressure in the ionization chambers was raised to 760 Torr. The singles spectra measured in the four detectors are given in Fig. I-88.

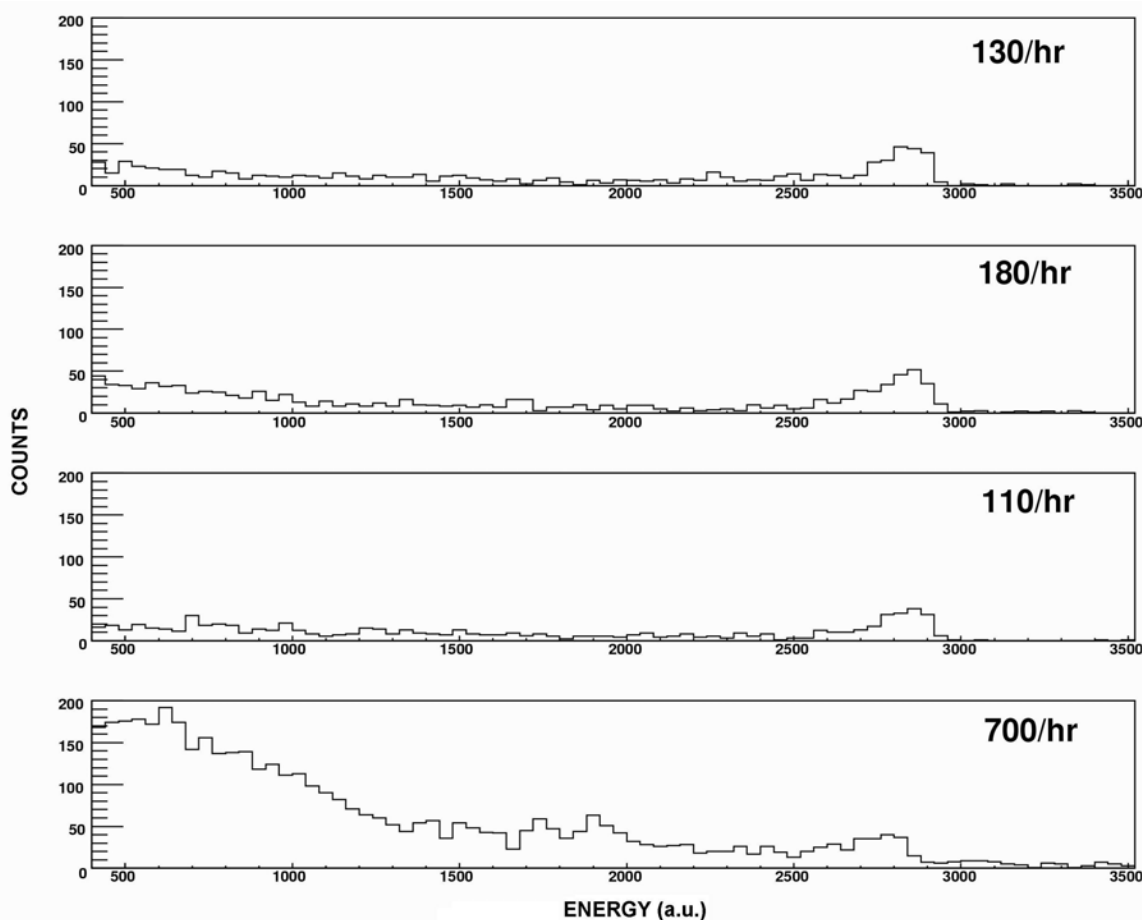


Fig. I-88. Background spectra measured in the four ionization chambers. The peak in the spectra originates from the alpha decay of ^{210}Po in the solder material. The pressure in the ionization chambers during these measurements was 760 Torr.

As can be seen from these results, the rates above the threshold of ~ 100 keV are about 150 particles/hour for three of the detectors, while the rate of the fourth detector is about five times this value. From the energy of the peak (5.2 MeV) and the higher count rate for detector 4, the origin of the background could be traced back to ^{210}Po which is produced via beta decay from ^{210}Pb present in the solder material used for the Frisch grid. This background is known from other low-count rate experiments which experienced an alpha background with a half life of 138 days. Since the Frisch grid of detector 4 had been re-ordered shortly before this measurement, a higher background was observed for this detector. The rate has since decreased by more than a factor of four and the background rates of the four detectors now approach 1-2 counts/minute. Another source of background originated from ^{16}N diffusing from the

irradiation region into the ion chambers. To eliminate this contribution all detectors have been surrounded with a thin layer of Teflon.

To test the sensitivity of the ionization chambers to beta particles, a ^{22}Na β^+ source with a strength of about 10^5 decays/s was mounted on the target wheel and positioned in front of detector 3. The energy spectra measured for the four detectors are shown in Fig. I-89. The count rates of these spectra, taken about 4 months after the ones shown in Fig. I-88 exhibit a decrease of the count rate in detector 4 by the expected factor of two. Detector 3, which faces a β source emitting about 5×10^4 into its active volume, only shows an increase in count rate of 60 counts/hr above the threshold of 100 keV. For a coincidence measurement this background rate is negligible.

*Hebrew University, Jerusalem, Israel, †Northwestern University, ‡University of North Carolina, §Western Michigan University.

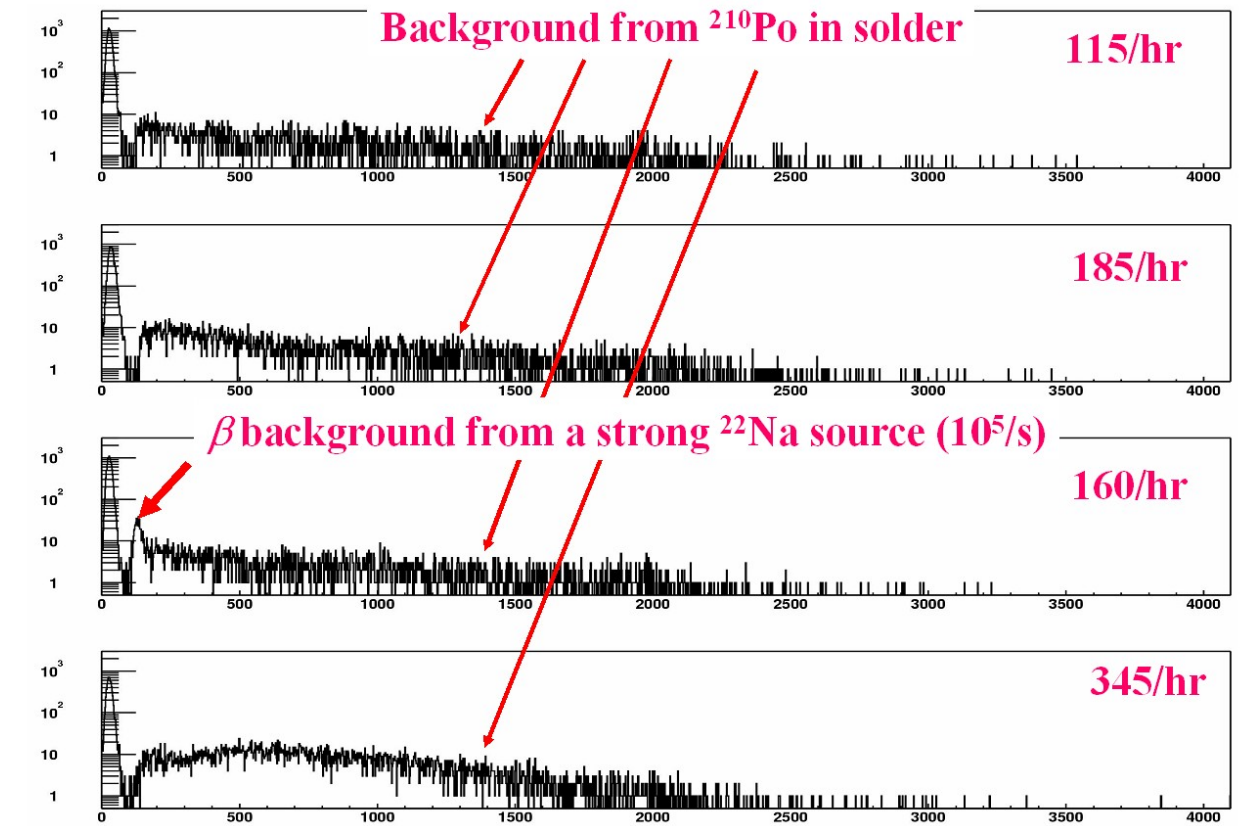


Fig. I-89. Test of the response of the ionization chambers to beta particles. A strong ^{22}Na source was facing detector 3. The main background (typically 200 counts/hour) is caused by the alpha decay of ^{210}Po . The pressure in the ionization chamber during these measurements was 150 Torr.

h.23. Simulation of the Detector Response in the ^{16}N β -Delayed α Decay Experiment (X. D. Tang, K. E. Rehm, and J. P. Schiffer)

In the study of the ^{16}N β -delayed α decay there are three effects that need to be investigated carefully:

- Alpha particles with energies down to 0.6 MeV have to be detected in coincidence with ^{12}C ions of even lower energies (~ 0.2 MeV). Any significant energy loss of the outgoing particles in the absorber foil will deform the shape of the spectrum. It is, therefore, crucial to minimize the energy loss and to reduce the electronic noise so that even the low-energy ^{12}C particles can be clearly identified.
- If a particle, emitted from the foil is stopped in the support frame, only a part of the energy is deposited in the gas. Such an event must be clearly separated from the good coincidences.
- The detection efficiency must be constant over the important alpha energy range from 0.6 MeV to 2 MeV.

A detailed Monte Carlo simulation program has been developed to investigate these effects. In the simulations, the theoretical alpha spectrum from

Ref. 1 was used to sample the decay. An example of a simulation in comparison with real events from a test run is shown in Fig. I-90. The ionization chamber was filled with P10 gas at a pressure of 150 Torr and the thickness of the absorber foil was $15 \mu\text{g}/\text{cm}^2$. The two main groups correspond to ^{12}C - α coincidences identified in detector 1-2 or 2-1, respectively. The third group, located in the vicinity of the origin, results from alpha particles that hit the target wheel and deposited only part of their energy in the P10 gas. Events between the two main peaks originate from gaseous ^{16}N particles that diffuse into the ionization chamber and deposit their energy in both detectors.

After varying the various geometrical parameters, the best experimental configuration was determined. For a beam spot with a diameter of 5 mm, we chose a $10 \mu\text{g}/\text{cm}^2$ thick carbon catcher foil mounted on a target frame with a thickness of 1.75 mm and a 10 mm diameter hole. In order to reduce the background from the diffusion of ^{16}N , the ion chambers were wrapped with Teflon foil. The simulations also provide an important input for a better understanding of the energy-angle relation obtained from the Frisch-grid and anode signals of the twin-ionization chamber and for the pressure dependence of the device.

¹R. E. Azuma *et al.*, Phys. Rev. C **50**, 1194 (1994).

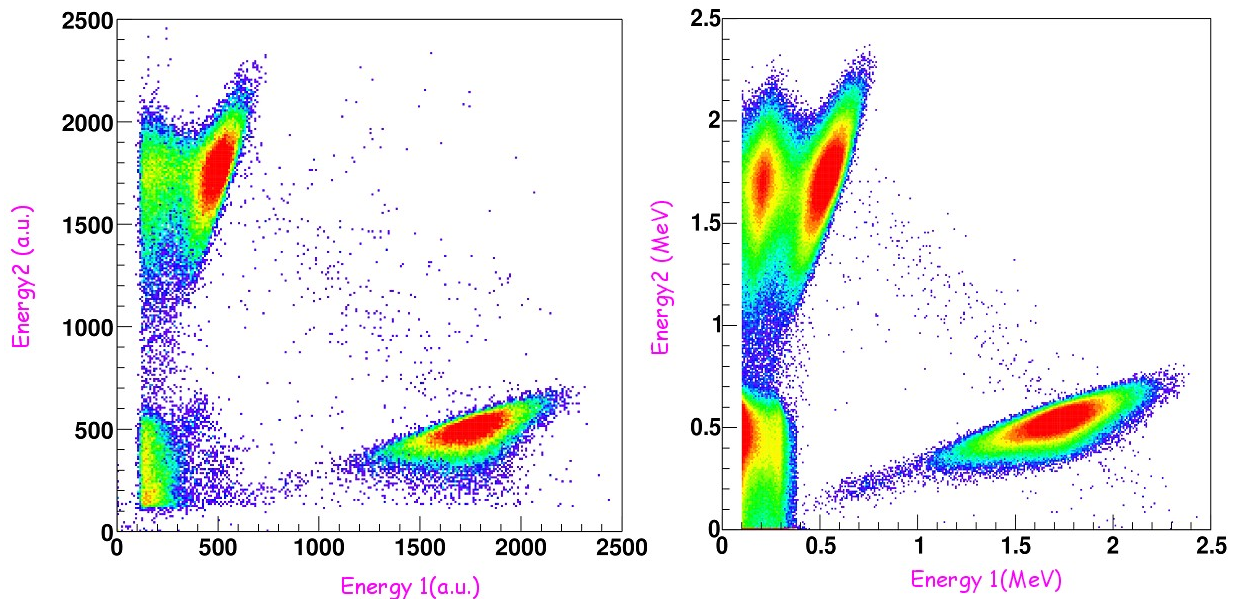


Fig. I-90. Left: Two-dimensional spectrum of ^{12}C -alpha coincidences measured in one of the twin-ionization chambers using a $10 \mu\text{g}/\text{cm}^2$ carbon foil that was irradiated with ^{16}N particles. Right: Monte Carlo simulation of the detector response using the actual geometry of the detectors.